General comments

Abstract : Try to group the sentences related to the background and those related to the methods to ease the reading. Highlight most relevant results, which are not only the evidence of a permafrost-free belt, but also outcome from the regression analysis and validation for example. Hint at the broad significance, not only « new information for users ».

We reordered some sentences referring to background and methods and added further content on the outcome of the study as you suggested.

Methods : I wonder about the relevance of presenting the « Mapping approach » before the regression analysis as it introduces concepts related to the regression (example of « the double standard error of our model output»). Some details are not necessary at this stage (example : « the buffer area was mapped in yellow ») and confuse the reader. At this stage of the method, it is in my opinion better to introduce the modeling approach rather than the mapping approach which is the final product and a way to express the model. Similarly, the regression approach is presented at the same time as the mapping approach (P4, L1-5) and it would be better to start from description L31 (P3) : explaining main predictors variables, then the regression analysis and finally the mapping approach. This is a suggestion, but in the current state, the method section is still confusing.

You are completely right. This problem was easy to solve. We moved the entire paragraph which deals with description of the final map product : "It includes all areas with modeled negative ground temperatures….. possible patchy permafrost" from the beginning of section 2.1 to the very end of section 2.1 where the actual mapping of zone 1 is described in the subsection "step 4: mapping zone 1".

In addition, there is one technical point which remains very unclear to me. In the methods (P4), it is stated that an aspect-dependent factor is used to account for long-wave solar radiation. Do the north faces receive such long-wave solar component ? Even though north faces have temperature close to the air temperature they remain warmer than the air. Why do the aspect-depend factor is 0 for North faces ? Wouldn't it be a way to account for this offset between air temperature and rock surface in shaded faces ?

We do not fully agree that MAGT in north faces always stay warmer than the MAAT. I just recently read about the example from Kitzsteinhorn:

"Mean annual crack top temperature(MACTT) was more than 1 °C lower (-3.3 °C) than MAAT in 2016."

https://www.the-cryosphere-discuss.net/tc-2019-42/tc-2019-42.pdf

The examples given in Haberkorn et al. 2015 show rock temperatures under snow free conditions, which are during the summer months slightly higher than the air temperatures. These values originate however from a WNW facing slope where our factor is > 0. A slightly negative annual radiation balance in steep snow free or snow poor rock slopes facing exactly north is considered by us as well as possible as a slightly positive radiation balance. Beyond that, the aspect dependent factor is of course just an approximation of the actual radiation balance in rock slopes.

In the step 1 you use a 2 m resolution DEM and in step 4 a 25 m DEM. Why not always using the best resolution DEM ? Can you explain your choices ?

Yes, this is simply because of the computing capacity and the size of the dataset. For small areas around the boreholes it is feasible to work with the high resolution DEM. When extrapolating our results to the entire Swiss Alps however, we had to switch to a lower resolution. We added a short explanation in the text.

Could you add a figure to illustrate Step 3 (regression results).

Yes, we added a figure to the supplementary material.

You propose a sensitivity analysis (P6) based on a « randomly bisected sample ». I wonder why not being aligned with former statistical studies and common statistical approach such as (Boeckli et al., 2012) using a 10-folds cross-validation . Wouldn't it provide more robust results ?

Well, what we proposed here was actually a 2-fold cross-validation. To access the robustness of the model, it seemed reasonable to shrink the training data by 50% instead of 10% as it is the case in a 10-fold cross validation. As you and the Editor were not happy with this approach, I changed to a 10-fold cross validation.

In your sensitivity analysis, you state that the PISR cannot provoke random changes in the regression results because it is based on same calculation. However, you assume some snow-cover areas for 6months, which might be very far from real-world situation with lower elevation getting snow free earlier than higher elevation. Considering the same « winter time » for all terrains might be a important limit in your approach and this might be explained and discussed.

Yes you are right here, although I would consider this as a systematic error of the model which has however little connection to the model's sensitivity. The latter rather represents a value for the stability of the model against (random) changes in the input data. We discussed this issue shortly in section 2.2

Results : This section is messy. Please divide in sub-sections, presenting results of the regression analysis, sensitivity analysis and then the map. It is a pity that the pattern of permafrost distribution is not better described but I understand that this is not the main message of the paper as reflected by the title. But giving a few statistics (min, max, mean elevation for example) for comparison with other maps would reinforce the results and would be interesting for the community. In my sense, it would strengthen the visibility of this paper.

We added 3 subsections:

3.1. Linear regression analysis of MAGT

3.2. Permafrost distribution in the PGIM

3.3 Validation of the permafrost maps

Furthermore we moved the histogram of permafrost distribution from the supplementary to the main manuscript. We gave some minimum elevations or ice-poor permafrost. Mean and max values are little meaningful in our opinion because they are controlled by topography (existing area per elevation zone).

Discussion : Section 4.4 is very poor. Either you develop a little bit more with examples showing how your map could support societal decisions and challenges, or you move these sentences in the introduction or perspective.

We have added information explaining why ice-rich substrates are problematic for the construction of mountain infrastructure and should thus be avoided during the planning of infrastructure. This underlines that a map indicating the presence of ice-rich permafrost is highly useful for engineers. Knowledge of permafrost temperatures is also useful in the choice of construction materials.

In section 4.5, I am quite doubtful about the application of your mapping approach with future climate scenarios. Your suggestion doesn't account for transient effect. The same is true for your mapping approach and this might be introduced in the methods and discussed in the discussion.

Yes you are right. We made supplements in two parts of the discussion:

4.1. "…Additional deviations might arise from the climate warming signal in the borehole temperatures. While surface near temperatures might be in accordance with the current climatic conditions, temperatures at greater depth are still influenced by previous decades with colder climate. As temperatures at several depth are included in our reference data set, depth dependent deviations can occur. Our model for ice-poor permafrost does thus not represent a permafrost distribution which is in equilibrium with the current climate conditions but a snapshot of the current distribution of ice-poor permafrost, which currently adapts to warmer climate conditions."

4.5. "…As for different climate regions, the elevation models can also be adapted to future scenarios of air temperatures. However, when adapting our results to a different climate, the transient effects have to be considered. As explained in 4.1. our model represents the actual current permafrost distribution in the Swiss Alps and is therefore not in equilibrium with the current climate. This disequilibrium might be smaller or larger in future or in different world regions."

P17 L17-19 : this is not clear what should be tested (other areas ? future scenarios ?) and what is in preparation. Please clarify.

Yes, thank you, this was ambiguously written. We rewrote it.

Detailed comment

P2 L9 : « a ground temperature dataset »

Thank you

P2 L20 : « to convert the energy balance results » sounds clumsy

Changed to: " to define a permafrost likelihood or index based on the energy balance results"

P3 L14-15 : list the processes again, maybe in brackets, but the reader has lost track of the above description when reaching that point.

We rewrote this sentence

P3 : sometimes you use « Zone », and sometimes « zone » : be consistent.

We adapted this.

P4 L15 : it is inaccurate to state that most alpine ground surface are snow-covered during 6 months. I would suggest using « winter time », since snow cover duration is highly dependent on elevation and aspect.

We changed to: during large parts of the year.

P4 L17 : could you just explain why you chose a threshold of 40° ? Based on which assumption or background ?¨

Yes we rewrote this section, gave a reference and some more explanations.

One problem is not discussed in the paper (hard to understand at this point of the paper and therefore confusing): As we work with two different DEM resolutions for model calibration and map production (2m and 25m) slope as well calculated over different extents. In the map, 40° refers to an average slope over 75 m. (This corresponds to the edge length of 3 raster cells of the used DEM. Slope is calculated over 3x3 cells of the DEM.) This implies that in most cases, there are clearly steeper parts within this area from which the snow slides off and accumulates in gullies or less steep parts. Especially in southern slopes this causes a positive feedback of exposed rock -> higher albedo -> warming -> snow melt in less steep parts of the slope. See your following remark below.

P4 L23 : which « feedback » are you talking about ?

This is explained in the following sentence. We added a colon behind feedback and explained the positive feedback in more detail.

P4 L24 : I do not understand, you are describing processes of rock walls and speak about « wet avalanche » ? Are avalanche really a typical process of rock walls ? I think that most of snow accumulating on rock walls melts away, but doesn't accumulate over substantial thickness and surface area to trigger avalanche. Could you clarify ?

We refer to both, melt and avalanching. Avalanches includes here all types of sliding snow. This may be less often a typical slab avalanche but smaller sluffs of wet snow or small gliding avalanches. They regularly occur in steep south facing terrain during large parts of the year, including warm winter days.

P6 L4 : remove « work » from « manner as in work step 1 ».

Ok

P7 L15-17 : what about permafrost forming in deglaciered rock walls (e.g. Wegmann et al., 1998) ?

Here we are in the section describing the methodical approach for zone 2 (ice-rich permafrost). There are per definition no rock walls in zone 2.

P7 L32 : what do you mean ? « The human polygon editor » The authors ? Not aware of the position of the validation points ???

The polygons were edited by Ilja Burn (Acknowledgements) and the first author. The editing task took place on the background of an orthophoto. During editing the editors did not know where the validation points were located and had therefore no incentive for an subjective editing of zone 2 at the locations with validation points. (In deed only a very few validation points were affected by editing and the editing task was quite unambitious at these sites, i.e. correcting some rock glacier outlines)

P8 L20 : what about talus slopes ? Are they considered ? Are some relevant data existing for validating the model ?

Talus slope permafrost is considered by the 92 validation points of which several lie in talus slope. As discussed later, there is a bias towards permafrost occurrence in these validation points. Permafrost absence in talus slopes is unfortunately underrepresented.

P15 L30-31 : it might be something missing in this sentence, not clear

This was actually a supplement to the previous sentence. It was unclearly written we corrected this.

P16 L15 : a « a » is missing in « permafrost »

We could not find the missing a? In our manuscript it was there??

P17 L5 : something wrong in the phrasing

I guess a comma was missing.

Additional Changes: We adapted the regression coefficients in Formula (4). The values in the last manuscript version originated from an old version of the map and were forgotten to change. We apologize this mistake.

Distinguishing ice-rich and ice-poor permafrost to map ground temperatures and ground ice occurrence in the Swiss Alps

Robert Kenner[1], Jeannette Noetzli[1], Martin Hoelzle[2], Hugo Raetzo[3], Marcia Phillips[1]

[1] WSL Institute for Snow and Avalanche Research SLF
[2] University of Fribourg, Department of Geosciences
[3] Federal Office for the Environment FOEN

Correspondence to: Robert Kenner (kenner@slf.ch)

Abstract. Mountain permafrost is invisible and mapping it is still a challenge. Available permafrost distribution maps often overestimate the permafrost extent and include large permafrost-free areas in their permafrost zonation. In addition, the representation of the lower belt of permafrost consisting of ice-rich features such as rock glaciers or ice-rich talus slopes can be challenging. These problems are caused by considerable differences in genesis and thermal characteristics between ice-poor permafrost occurring for example in rock walls, and ice-rich permafrost. While ice-poor permafrost shows a strong correlation of ground temperature with elevation and potential incoming solar radiation, ice-rich ground does not show such a correlation. Instead, the distribution of ice-rich ground is controlled by gravitational processes such as the relocation of ground ice by permafrost creep or by ground ice genesis from avalanche deposits or glacierets covered with talus.

We therefore developed a mapping method which distinguishes between ice-poor and ice-rich permafrost and tested it for the entire Swiss Alps. For ice-poor ground we found a linear regression formula based on elevation and potential incoming solar radiation which predicts borehole ground temperatures at multiple depths with an accuracy higher than $0.6°$ C. The zone of ice-rich permafrost was defined by modelling the deposition zones of alpine mass wasting processes. This dual approach allows the cartographic representation of permafrost-free belts, which are bounded above and below by permafrost. This enables a high quality of permafrost modelling, as is shown by the validation of our map. The dominating influence of the two rather simple connected factors elevation (as a proxy for mean annual air temperature) and solar radiation on the distribution of ice-poor permafrost is significant for permafrost modelling in different climate conditions and –regions. Indicating temperatures of ice-poor permafrost and distinguishing between ice-poor and ice-rich permafrost on a national permafrost map provides new information for users.

1

1 Introduction

Maps of potential permafrost distribution are useful products applied in different fields of practice and research because permafrost is an invisible subsurface phenomenon. Such maps are used to plan construction work in alpine terrain, to evaluate local slope instability or to estimate large-scale permafrost occurrence for scientific purposes. Mapping permafrost in the highly variable alpine landscape is however challenging, particularly on a global scale where ground temperature data or climate and terrain datasets are rare (Fiddes et al., 2015; Gruber, 2012). Developing a method appropriate to model mountain permafrost therefore requires test areas with a dense set of reference and validation data, as well as highly resolved digital terrain models. The Swiss Alps are an ideal test site, as various research activities during the last decades provide a ground temperature dataset, which is largely included in the Swiss permafrost monitoring network PERMOS (2016). Consequently, many authors have used the Swiss dataset to calibrate or validate their permafrost distribution model (Böckli et al., 2012; Deluigi et al., 2017; Fiddes et al., 2015; Gruber et al., 2006; Gruber and Hoelzle, 2001; Haeberli et al., 1996; Hoelzle et al., 2001; Keller, 1992; Keller et al., 1998).

The core of these models is a more or less simplified surface energy balance. Typically, mean annual air temperature (MAAT), represented by elevation and potential incoming solar radiation (PISR) are basic parameters (Hoelzle and Haeberli, 1995). Some authors only use MAAT (Azócar Sandoval et al., 2017) or freezing degree-days and snow cover (Gisnås et al., 2017; Ishikawa, 2003) as external forcing parameters. Fiddes et al. (2015) also consider precipitation and in particular snow cover, wind, humidity and a complete surface radiation balance in a purely physics-based method. Most other studies however used empirical-statistical approaches to define a permafrost likelihood or index based on the energy balance results and in dependency of landforms, surface coverage, vegetation or topographic characteristics such as slope or curvature (Böckli et al., 2012; Deluigi et al., 2017; Gruber, 2012; Hoelzle et al., 1993).

However, the actual distribution of mountain permafrost includes phenomena which cannot be sufficiently explained using surface energy balances. This mainly concerns the existence of excess ground ice at the base of talus slopes or in rock glaciers (Haeberli, 1975), which often occur hundreds of metres below the zone of continuous permafrost and are surrounded by permafrost-free ground. This type of permafrost, hitherto referred to as ice-rich permafrost, sometimes exists at locations with higher annual surface heat fluxes than in the surrounding permafrost-free areas (Lerjen et al., 2003; Scapozza et al., 2011). The permafrost-free belts between the ice-rich permafrost at lower elevations and permafrost with lower ice contents at higher elevations are not reproduced in the existing large scale mountain permafrost maps, as was highlighted by Lerjen et al. (2003) and Scapozza et al. (2011). This is because thermally defined maps have no information on ground ice content.

Ice-rich permafrost can persist under warmer climate conditions than ice-poor permafrost due to the high heat capacity of ice (Scherler et al., 2013). Due to latent heat effects, active layer thickness deepening was less pronounced in ice-rich permafrost than at ice-poor monitoring sites in the Swiss Alps during the last two decades (PERMOS, 2016). However, if active layer thickening did occur, it was reversible in ice-poor permafrost (Hilbich et al., 2008; Krautblatter, 2009; Marmy et al., 2013), but irreversible in ice-rich permafrost due to the melt of considerable amounts of ground ice (Zenklusen Mutter and Phillips, 2012). This highlights ground ice as a requirement for the existence of permafrost at ice-rich, low-elevation sites. It is therefore a logical step to

2

consider the ice content when mapping permafrost distribution, just as it is done for physics-based permafrost modelling (Hipp et al., 2012; Pruessner et al., 2018; Staub et al., 2015).

The differentiation between ice-rich and ice-poor permafrost was performed indirectly in earlier studies by including concave footslope positions in permafrost distribution models (Ebohon and Schrott, 2008; Keller, 1992). The permafrost and ground ice map (PGIM) presented here aims to reproduce the elevational permafrost gap by providing a better delimitation of the two main types of permafrost in alpine terrain. We consider the distribution of the continuous zone of ice-poor permafrost (permafrost without excess ice) as being mainly controlled by the surface energy fluxes. While negative temperatures allow small amounts of persistent ground ice in ice-poor permafrost, we assume the opposite for the ice-rich permafrost: Here, the ground ice enables the existence of permafrost, decoupled from current atmospheric conditions and often protected by coarse talus at the surface (Scherler et al., 2014; Schneider et al., 2012). The origin of this ground ice can be syngenetic due to the burial of snow and surface ice by rock debris (Haeberli and Vonder Mühll, 1996; Kenner, 2018) or epigenetic if originating from colder climate periods and displaced by long term rock glacier creep (Haeberli, 2000). To include both ice-poor and ice-rich permafrost in our map, we consider the surface energy balance in our model, which is decisive for the distribution of ice-poor permafrost. We also consider ground ice formation and relocation due to mass wasting processes, which control the distribution of ice-rich permafrost.

2 Methods

The permafrost and ground ice map (PGIM) of Switzerland distinguishes two alpine permafrost zones: zone 1 indicates modelled ground temperatures and is based on the parameters elevation and PISR. Zone 2 indicates areas outside of zone 1 which might be categorized as permafrost due to the existence of excess ground ice. The modelling approach for zone 2 differs fundamentally from that of zone 1: whereas zone 1 considers thermal conditions, the potential existence of ground ice is considered in zone 2; either due to superimposed rock fall and snow avalanche deposits or due to the gravity-driven relocation of excess ground ice.

2. 1 Mapping approach for zone 1

Zone 1 of the PGIM was derived from modelled ground temperatures. The ground temperatures were calculated based on a multiple linear regression analysis using the explanatory variables PISR and elevation (as a proxy for mean annual air temperature). These are the two most important parameters for the surface energy balance (Hoelzle et al., 2001) and are used in almost all permafrost distribution models. Ground temperatures measured in 15 reference boreholes were used as predictor variables. These boreholes were chosen from areas without ice-rich permafrost in Switzerland and Italy, close to the Swiss border (upper 15 sites in table 1). Temperature is measured by thermistors in the boreholes at multiple depths between 15 and 100 m with a sub-daily temporal resolution. The thermistors commonly have a measurement accuracy of around 0.1°C or better, and the types of thermistor and data loggers are specified in PERMOS (2016).

The basic concept was to attribute a PISR value, an elevation value and a mean annual ground temperature (MAGT) to each of the 212 thermistors. Based on this dataset, the regression parameters a, b and c in formula 1

3

Gelöscht: all

Gelöscht: processes described above

Gelöscht: .

Gelöscht: Zone

Gelöscht: It

[1] nach unten: includes all areas with modelled negative ground temperatures and a buffer area with ground temperatures ranging between 0°C and 1°C. This buffer of 1 K corresponds to about the double standard error of our model output. The area of zone 1 with negative ground temperatures was labelled "Permafrost" and mapped in blue colours. The buffer area was mapped in yellow and is described as "possible patchy permafrost".

Gelöscht:

were determined and later used in formula 4 to calculate the ground temperatures in zone 1. The four detailed work steps involved are explained below.

$$(1) \qquad MAGT = a + b \cdot R + c \cdot E$$

Where:

5    $MAGT$ is the mean annual ground temperature measured by each individual borehole thermistor

R is the solar radiation value for each individual thermistor

E is the elevation value for each individual thermistor

Step 1: calculating solar radiation values for the ground surface

PISR at the ground surface around each borehole was calculated using the ESRI tool "Area solar radiation". The
10 processing was based on a digital elevation model with 2 m resolution (swisstopo swissALTI3D). The input parameter transmissivity was set at 0.4, and the diffuse proportion at 0.5, which corresponds to values recommended for moist temperate climates by the software developer. Most of the alpine ground surface is snow-covered during large parts of the year and receives no insolation during that time. However, steep areas such as rock walls remain snow-free for the entire year (Magnin et al., 2015). To consider the snow cover in
15 slopes below 40°, we only used PISR values calculated for the generally snow-free period June to November (formula 2.1).

For slopes exceeding 40° we additionally included the winter solar radiation. This slope threshold lies within the zone in which winter snow cover clearly decreases (Pogliotti, 2011). Especially in sunny slopes, steeper than 40° C, winter insolation causes a positive feedback: Firstly, it causes snow removal due to melt or the triggering of
20 wet snow slides and subsequently an effective heating of the bare ground above the mean air temperatures (Haberkorn et al., 2015a). This in turn accelerates melt of the remaining snow. In steep, shady slopes however, winter insolation is often not strong enough to remove snow. In extremely steep parts in which snow cannot accumulate, long-wave radiation emission largely compensates the small amounts of incoming solar radiation in north facing slopes. This causes rock surface temperatures close to the air temperatures (Haberkorn et al., 2015a).

25 Our simplified model does not consider the emission of long-wave radiation and any additional winter insolation leads to a warming of the ground on an annual basis. As described above, this might be correct for southern slopes but not for northern ones. To overcome this weakness, the winter insolation (December to May) which affects the steep terrain parts was multiplied with an aspect-dependent factor. This factor ranges between 0 for the azimuth North (no effect of winter insolation due to similar strong long-wave emission) and 1 for the
30 azimuth South (strongest effect of winter insolation due to snow removal). The winter solar radiation was then added to the summer solar radiation values and applied to slopes steeper than 40° (formula 2.2).

For slopes < 40°:   (2.1) $r = PISR_{June-Nov}$

For slopes > 40°:   (2.2) $r = PISR_{June-Nov} + PISR_{Dec-May} \cdot A$

Where:

35   r is the solar radiation value at a single surface point

PISR   is the potential incoming solar radiation

A   is an aspect factor ranging from 0 (N) to 0.5 (E/W) and 1 (S)

4

Step 2: attributing solar radiation and elevation values to each borehole thermistor

To attribute PISR and elevation to a thermistor we created a point cloud with 2 m resolution, representing the ground surface around each borehole. Every point contained information on its elevation and PISR. Radiation and elevation values for all surface points surrounding a thermistor influence its MAGT. To aggregate all these values into one radiation and elevation value representative for a thermistor, a spatial average was calculated (formula 3, as for elevation). The closer a surface point is to a thermistor, the stronger its influence. This was considered by an inverse distance weighting (factor d in formula 3). The larger the distance between a thermistor and a surface point, the higher the number of points lying within this distance. This increases the weight of distant surface areas when calculating a spatial average. To avoid this we categorized all points into distance classes with a 1 m increment, and included a second weighting factor considering the number of points within one distance class (factor k in formula 3). The maximal distance considered was 5 times the minimal distance of the thermistor to the ground surface. This factor was parameterised empirically by minimalizing the sum of residuals between measured and modelled ground temperatures.

$$(3) \qquad R = \frac{\sum_{i=n}^{i=1} d_i \cdot r_i \cdot k_i}{n}$$

Where:

R is the solar radiation value defined for each individual borehole thermistor

n is the number of distance classes

d is a weighting factor which considers the distance between a surface point and the thermistor (inverse distance weighting)

k is a weighting factor which considers the number of surface points within one distance class

r is the solar radiation value of a single surface point

Step 3: Setting up the regression model

We analysed the dataset of step 2 in a multiple linear regression corresponding to formula 1. Naturally, the measured MAGT of a single thermistor deviates from the regression line towards warmer or colder conditions. This spread indicates the occurrence of permafrost in places where the regression result indicates slightly positive temperatures. The intention of the PGIM was rather to accept permafrost free areas within permafrost zone 1 than to include permafrost areas outside of zone 1. To include deviations towards lower temperatures in zone 1, the regression analysis was carried out twice. While all thermistors were used in the first iteration, only those thermistors with a measured MAGT below the modelled MAGT in the first iteration were used in the second iteration. Step 3 is summarized in Figure A (Supplementary Material).

5

Step 4: mapping zone 1

To map zone 1, the defined regression parameters a, b, and c were applied to a digital elevation and insolation model with 25 m resolution (DEM25 and DIM25, based on the swisstopo DHM25). Due to file size and computing limitations, we had to decrease the resolution of the gridded datasets compared to step 1. Beyond that, the DIM25 was produced in the same manner as in step 1. The temperature value of each 25 m raster cell of the PGIM was defined by:

(4) $\quad MAGT_{PGIM} = 19.497 + 4.532 \cdot 10^{-6} \cdot DIM25 - 0.008043 \cdot DEM25$

Depth-dependent 3D effects (Noetzli and Gruber, 2009), which were considered by the inverse distance weighting in our regression model, are not included in our map. In fact, such effects lose significance due to the lower resolution of the map, where insolation variations are spatially averaged within a 25 m raster cell. The temperatures on the map can therefore be interpreted as representing roughly the spatial average of mean annual ground temperatures in a cube with 25 m edge length: this corresponds to the horizontal extent of a raster cell and the typical depths of our reference data boreholes.

Zone 1 includes all areas with modelled negative ground temperatures and a buffer area with ground temperatures ranging between 0°C and 1°C. This buffer of 1 K corresponds to about the double standard error of our model output. The area of zone 1 with negative ground temperatures was labelled "Permafrost" and mapped in blue colours. The buffer area was mapped in yellow and is described as "possible patchy permafrost".

2.2 Sensitivity analysis of the regression result

The regression result depends on the following parameters: PISR, elevation and reference MAGT. Changes in these parameters will influence the regression result. Elevation is independent from external influences and therefore uncritical for the result. Reference MAGT can be influenced by environmental conditions as well as by measurement errors, which are not considered here. Our small to medium size statistical sample of measured ground temperatures might be distorted in comparison to the total statistical population. To test the sensitivity of our result to changes in the statistical sample, we carried out a 10-fold cross validation by randomly splitting the reference MAGT into 10 samples, nine of which were used as training data for our regression model and one as test data. The validation was carried out 10 times with each of the 10 samples as test sample, subsequently the resulting MAGT deviations of all 10 runs were averaged. The calculation of PISR values, especially in steep terrain, included several other parameters such as the distance threshold, a slope threshold, an aspect-dependent weighting factor and assumptions for the timing of snow coverage. Indeed, the model was optimized by applying these parameters. The PISR values are however not an independent statistical unit of a sample of observations but are all based on the same calculation. This means that they can introduce systematic errors to the model, e.g. due to simplified assumptions of the snow cover timing, but they are not the origin of random changes in the regression result.

2.3 Mapping zone 2

Zone 2 includes all forms of ice-rich permafrost such as rock glaciers or ice-rich talus slopes. Therefore, we defined areas in which the burial of ice or snow by rock fall can lead to the development of ground ice or in

6

which epigenetic ground ice may have been relocated due to ice creep. We carried out 9 work steps, as shown in Figure B (supplementary Material):

1. Avalanche snow and rock fall deposits were assumed to accumulate at the foot of slopes steeper than 40°. Potential locations of deposits were modelled by calculating runoff tracks from such slopes using ESRI ArcGIS with a 25 m DEM (Supplementary Figure B, a) This was done in areas above 2000 m a.s.l., as only few, azonal permafrost sites exist below in the Alps (e.g. Cremonese et al., 2011).

2. The runoff tracks were buffered by a 120 m wide belt as shown in supplementary Figure B, b. In their upper parts, the resulting areas correspond to the main tracks of snow avalanches and rock fall. Further downslope they represent potential rock glacier creep paths. The buffer was wide enough to include particularly broad rock glacier tongues.

These areas were then reduced stepwise by excluding spatial intersections with other datasets through:

3. Removal of all areas steeper than 30° (Supplementary Figure B, c), which barely contain ice-rich permafrost (Kenner and Magnusson, 2017). Snow avalanches seldom form deposits in such steep slopes and epigenetic segregation ice in talus slopes would creep downslope.

4. Removal of all vegetated areas (Supplementary Figure B, d) because they commonly consist of fine-grained soils at relatively low elevations, where ice-rich permafrost is generally absent in the European Alps (Hoelzle et al., 1993). Vegetation cover was deduced from orthophotos ("SWISSIMAGE" provided by swisstopo) using the SAVI Index (Huete, 1988). Vegetated/unvegetated areas within the resulting 25 m grid were homogenized by iteratively applying a classic 3x3 cell erosion and dilation operation.

5. Removal of maximal extents of Little Ice Age (LIA) glaciation (Supplementary Figure B, e), because glacier coverage is known to disrupt underlying permafrost (Reynard et al., 2003; Ribolini et al., 2010). This dataset was created by Maisch (1999).

6. Removal of lakes and glaciers (based on "swissTLM3D" provided by swisstopo) (Supplementary Figure B, e)

7. Removal of flood plains, which were defined as being areas with slope < 4° and intersected by rivers (based on "DHM25" and "swissTLM3D" provided by swisstopo).

8. The remaining polygons were then aggregated to fill small gaps, simplified and smoothed. After this, all areas listed above were again excluded from the reworked polygons (Supplementary Figure B, f) .

9. Zone 2 can overlap zone 1 and zone 1 was mapped with the higher priority, which implies that ice-rich permafrost can also occur within zone 1, where it is not distinguished from ice-poor permafrost.

In a final step, the resulting polygons were checked and manually edited if necessary. Some still contained areas in which surface bedrock excludes the development of ice-rich permafrost. In a few cases, parts of rock glaciers were missing due to errors in the reproduction of creep paths or due to small terrain steps steeper than 30°. Manual editing included two tasks: All areas showing a bedrock surface, infrastructure or > 50% vegetation cover (for some reason not captured by the SAVI index) were removed from zone 2. Missing parts of rock glaciers were added to zone 2 if at least parts of them were already captured by the automatic mapping approach. An exemplary editing task is shown in supplementary Figure C. The human polygon editor was not aware of the positions of the validation points during this process.

7

2.4 Validation

Using the same validation dataset, we validated the PGIM and two other permafrost maps of Switzerland in addition to compare the results: The Alpine Permafrost Index Map (APIM) created by Böckli et al. (2012) and the Potential Permafrost Distribution Map (PPDM) (Gruber et al., 2006), available online in the swisstopo web map service (swisstopo, 2018). A more detailed methodical background to the PPDM can be found in Haeberli (1975), Keller (1992) and Gruber et al. (2004). The permafrost maps were validated using a set of 98 evidence points of permafrost occurrence or absence, of which 10 represent the Swiss reference boreholes used to set up the regression model for PGIM zone 1 (Table 2). The reference boreholes are distinguished from the other records in the PGIM validation results. A more detailed verification, e.g. of modelled temperatures, was not possible due to the lack of data. The validation dataset partly consists of records collected by Cremonese et al. (2011), of which we only used direct evidence of permafrost occurrence or absence having exact coordinates. Further validation points were provided by continuous near ground surface temperature data (GST) measured at 38 automatic weather stations in the Swiss Intercantonal Measurement and Information System (IMIS) (Russi et al., 2003). To balance the number of permafrost and permafrost-free validation points, only IMIS stations above 2400 m a.s.l. were used, which mostly lie within the critical elevation belt of discontinuous permafrost. The IMIS stations measure near-surface ground temperature at 10 cm depth with a Campbell 107 temperature probe. Of these 38 IMIS stations, 33 register a constant zero curtain during winter and are therefore expected to be on permafrost-free ground (Hoelzle, 1992). The remaining 5 stations show quite constant winter GST between -3°C and -4°C and are located on active rock glaciers. They were therefore classified as permafrost sites. A few additional validation sites were added from different sources (Table 2).

All classes of the PGIM were attributed with the number of validation records lying within them indicating permafrost occurrence or permafrost absence. Additionally, zone 2 of the PGIM was validated against an inventory of 124 rock glaciers in the Albula Alps created by Kenner and Magnusson (2017).

3 Results

3.1 Linear regression analysis of MAGT

Predicting the ground temperatures of the ice-poor reference boreholes on the basis of elevation and PISR yields a correlation coefficient of 0.94 and a standard deviation of 0.58°C (Table 3, Figure 1). This highlights the strong dependency of ice-poor permafrost on these two factors and its relatively high predictability. Including ice-rich permafrost in this regression analysis causes a drastic drop of the correlation coefficient and thus in the predictability of permafrost (Table 3 and Figure 2).
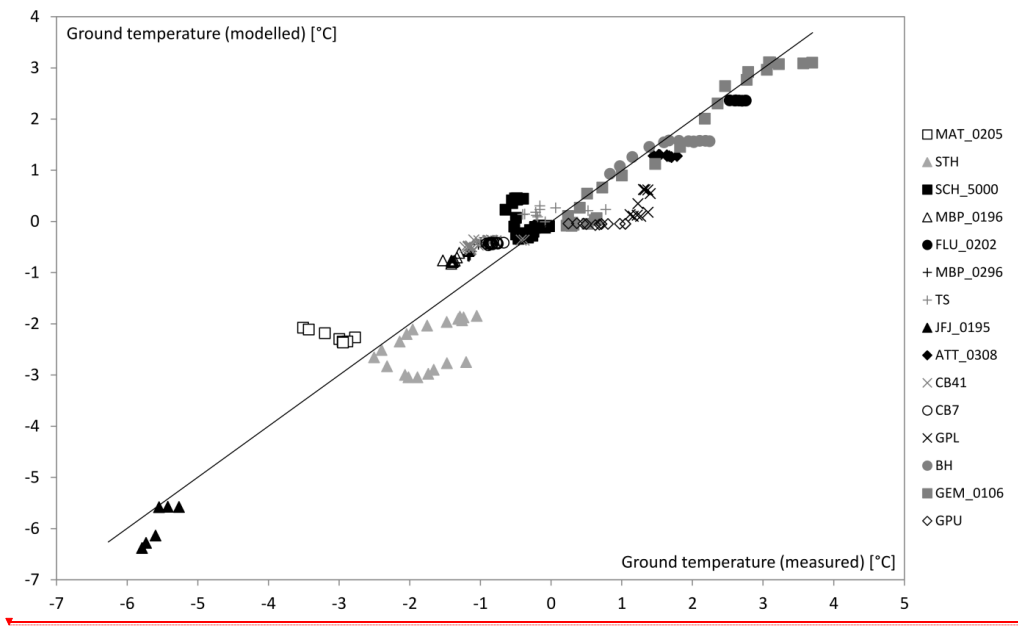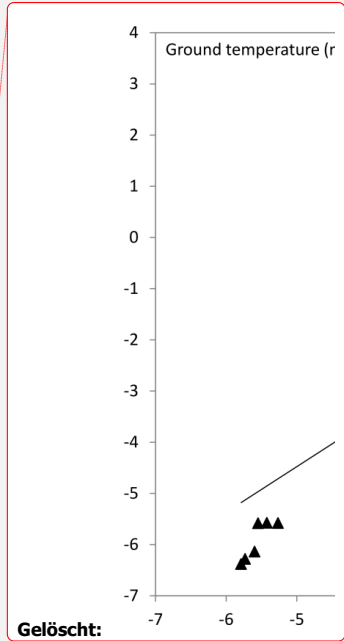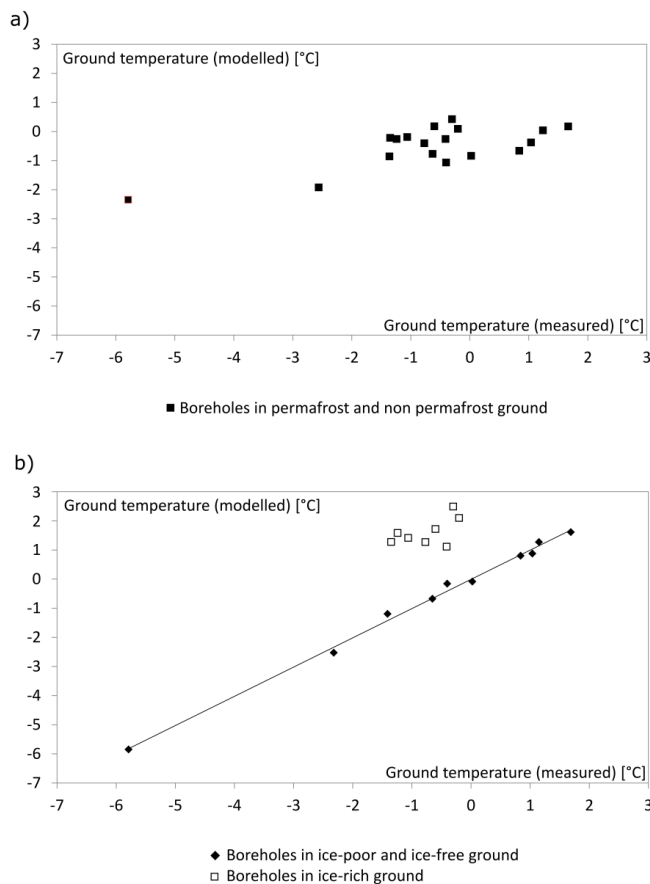
Gelöscht: error

Gelöscht: 57

Figure 1: Measured MAGT in 15 boreholes plotted against the modelled MAGT at the same locations. The regression line corresponds to formula (4) given in section 2.1. The borehole abbreviations are explained in table 1.

Although thermistors of individual boreholes show clear deviations from the regression line, the cross-validation indicates a high robustness of the regression analysis result. The standard deviation between the modelled and measured ground temperatures stayed constant at 0.58 °C. The MAGT calculated during the cross validation differed from the MAGT calculated based on the entire set of reference temperatures by a mean value of -0.003° C and a standard deviation of 0.025 °C. The highest deviation found for a single thermistor was 0.14° C. Explanations for the deviations of single boreholes or thermistors are presented in chapter 4.1.

9

a)

■ Boreholes in permafrost and non permafrost ground

b)

◆ Boreholes in ice-poor and ice-free ground
☐ Boreholes in ice-rich ground

Figure 2: Each data point represents a borehole and its measured and modelled mean annual ground temperatures at the depth with lowest temperatures. Included are the ice-poor boreholes 1-10 and all ice-rich boreholes in Table 2. The linear regression based on elevation and PISR shows no systematic relation between these two parameters and the ground temperatures when using both ice-poor and ice-rich boreholes for the regression (a), but a clear correlation appears when using only ice-poor or ice-free boreholes (b).

3.2 Permafrost distribution in the PGIM

An example section of the PGIM is shown in Figure 3. The entire map is available online as a shapefile https://doi.org/10.5281/zenodo.1470165. Together, zones 1 and 2 indicate a potential permafrost area (area considered by the map to potentially contain permafrost) of 2000 km^2 in the Swiss Alps, which is considerably less than that indicated by the APIM (3710 km^2 (Böckli, 2013)) and also less than on the PPDM (2550 km^2 (Gruber et al. 2006)). To estimate the actual permafrost area (area effectively containing permafrost), Böckli (2013) considered all areas of the APIM with an index value > 0.5. This results in an area of 2160 km^2 for the APIM. The PGIM includes 830 km^2 in the core area of zone 1 and 600 km^2 in zone 2, of which maximum 90% are expected to include permafrost according to the validation output. This results in an actual permafrost area of < 1400 km^2 in the Swiss Alps, which corresponds to < 3.4% of the area of Switzerland. For comparison, Keller et al. (1998) gave a value of 4-6 %.

Gelöscht: Although thermistors of individual boreholes show clear deviations from the regression line, bisecting the set of reference temperatures in ice-poor ground only had a small effect on the regression result. The differences between the modelled ground temperatures based on the entire set of reference temperatures and the ground temperatures based on the bisected sample showed a mean value of -0.11° C and a standard deviation of 0.15 °C. The highest deviation found for a single thermistor was 0.51° C. The similar values for the standard deviation and the mean value suggest that the changed reference sample mainly caused a constant offset of the temperatures of slightly over -0.1° C. This corresponds to an elevation shift of zone 1 by about 12 m

[2] nach oben: . Explanations for the deviations of single boreholes or thermistors are presented in chapter 4.1. ¶

Feldfunktion geändert

Formatiert: Englisch (Großbritannien)

The permafrost distribution over elevation is shown in Figure 4 for different aspects. In very shady, north facing slopes, ice-poor permafrost occurs down to around 2550 m a.s.l. In south facing slopes, ice-poor permafrost terrain generally starts about 350 m higher. Ice-rich permafrost can occur in all aspects and has no sharp lower boundary. While the map indicates the highest frequency of ice-rich permafrost slightly above 2500 m a.s.l. for slopes facing northwest to northeast, it is at around 2600 m a.s.l. for slopes facing southeast to southwest.
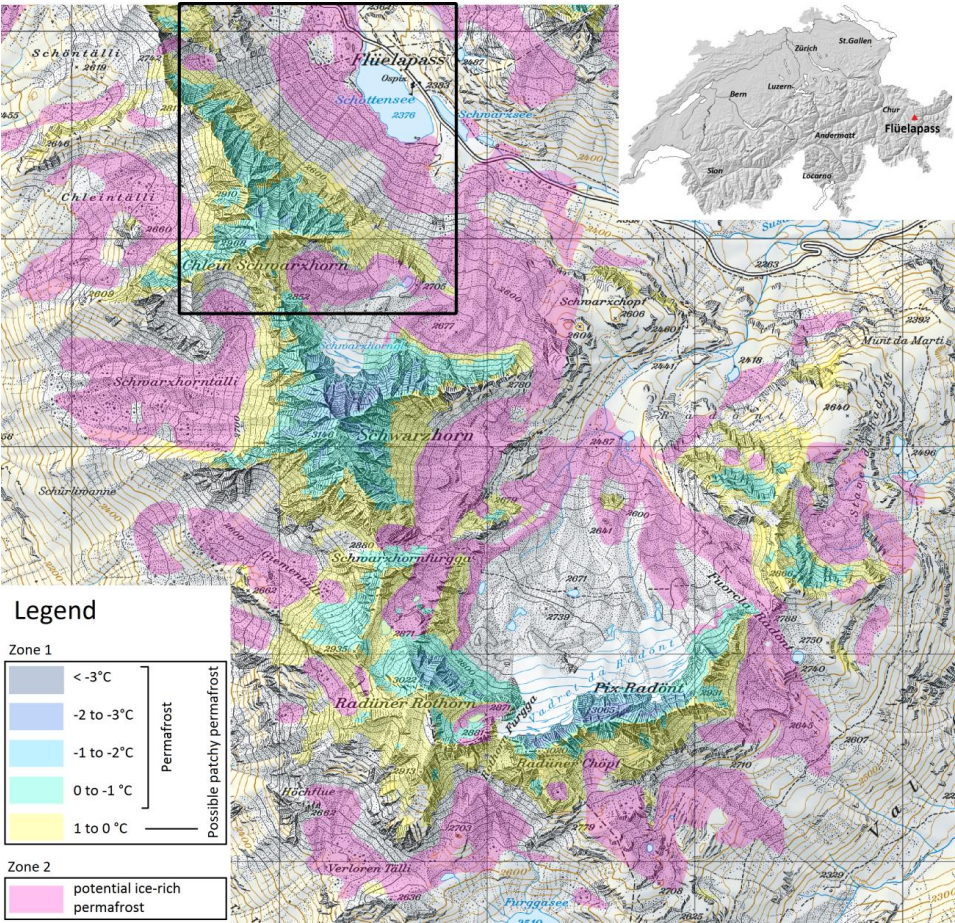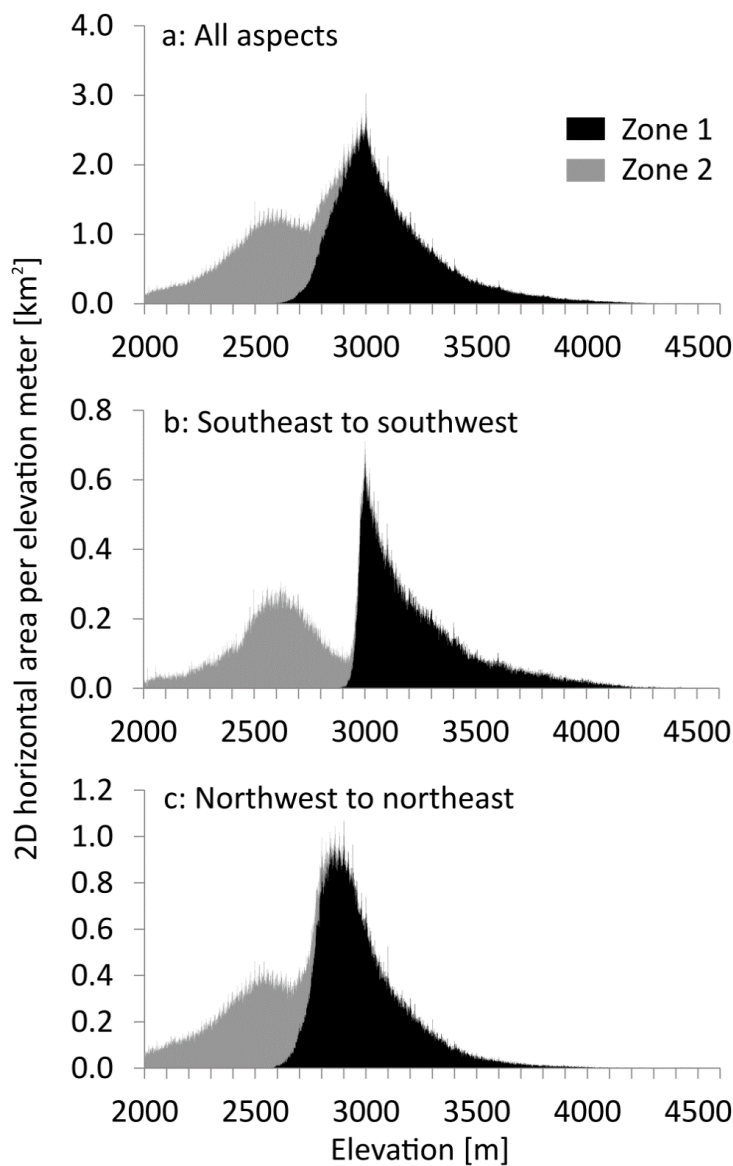
5

Figure 3: Map section of the PGIM close to Flüelapass in the Eastern Swiss Alps (inset map of Switzerland), showing the permafrost distribution in two zones. The black frame is the sector shown in Figure 9. The map grid has a resolution of 1 km. (Map: pixmaps © (2017) swisstopo (5704 000 000))

10

Gelöscht: 8

11

3.3 Validation of the permafrost maps

The validation of the PGIM (Figure 5) confirms the high accuracy of zone 1. Only two validation sites representing ice-poor permafrost are located outside the core area of zone 1 labelled "permafrost" (Figure 5). In turn, no permafrost-free sites were located in the core area of zone 1. Zone 2 (potential ice-rich permafrost) includes 21 sites indicating permafrost and 2 indicating permafrost absence. Zone 2 furthermore includes 95.5%

12

of the rock glacier area registered in the Albula Alps inventory (Kenner and Magnusson, 2017). This value applies to the automatically created version of zone 2 before it was manually edited.

The validation of the APIM (Boeckli et al. 2012) is shown in Figure 6. The zones with a permafrost index of 0 (no permafrost) or 1 (definite permafrost) have a similar error rate as the corresponding classes in the PGIM, but contain less validation records. The indices between 0 and 1 contain a rather homogeneous ratio of permafrost and no-permafrost sites, an increase in permafrost frequency is only visible for the very highly indexed areas (> 0.8).

The validation result of the PPDM (Gruber et al. 2006) is shown in Figure 7. The different probability ranges reflect the actual permafrost frequency quite well for the high probability classes but show larger deviations for the lower classes. Several permafrost evidence points exist outside the permafrost zonation of this map.
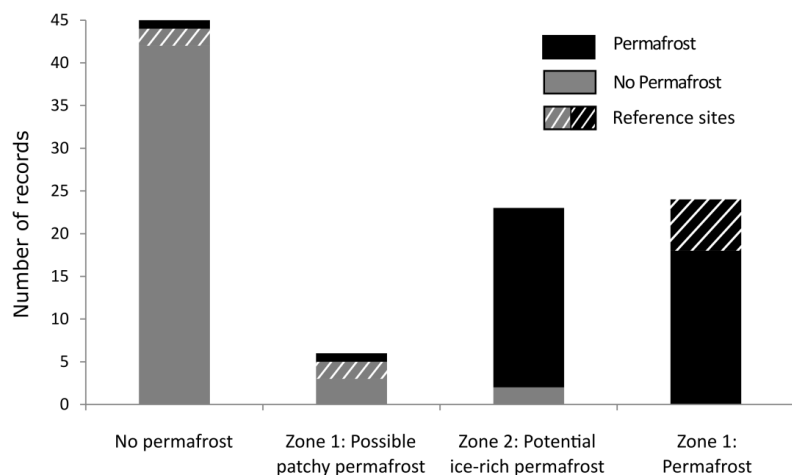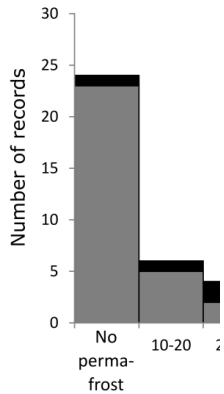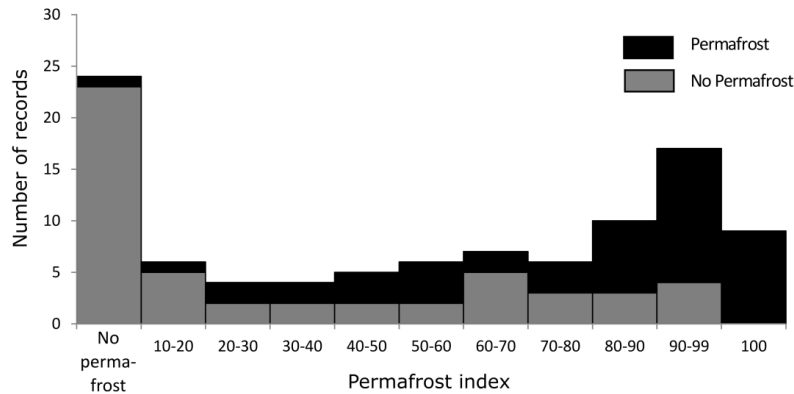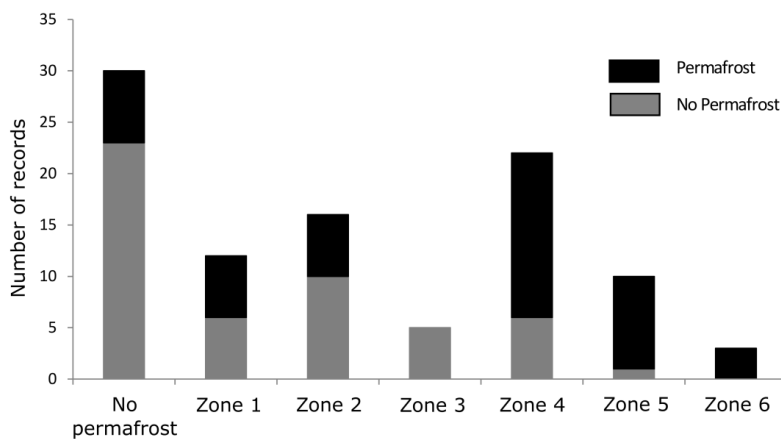
Figure 5: Validation of the PGIM showing the number of validation points with permafrost occurrence and permafrost absence in each map class. The striped sites represent the boreholes used to set up the regression model for the PGIM.

13

Figure 6: **Validation of the APIM (Boeckli et al. 2012) showing the number of sites with permafrost occurrence and permafrost absence for different permafrost probability ranges. As the map does not define classes but gives unique index values for each cell of the map, ranging from 0.1 to 1, these values were classified in 10 permafrost classes and a "No permafrost" class including all records outside the permafrost zonation.**

Figure 7: **Validation of the PPDM (Gruber et al. 2006) showing the number of sites with permafrost occurrence and permafrost absence in each map class. The zones were originally defined as follows: Zone 1 – local permafrost possible, patchy, discontinuous; Zone 2 - local permafrost possible, frequent patchy distribution; Zone 2 - local permafrost possible, patchy to extensive; Zone 4 – Extensive permafrost likely; Zone 5 – Extensive permafrost likely, increasing thickness; Zone 6 – Extensive permafrost likely, very thick in places, to over 100 m. The class "No Permafrost" includes all records outside the permafrost zonation.**

4 Discussion

4.1 Permafrost predictability

While the permafrost modelling based on the regression analysis was successful for ice-poor permafrost, it is not applicable for ice-rich permafrost (table 3). This makes ice-poor permafrost much better predictable than ice-rich permafrost. The high correlation coefficient achieved by the regression analysis is remarkable, because the borehole temperatures represent different landforms with strong differences in substrate and snow coverage. These factors, which influence ground temperatures (Haberkorn et al., 2015b; Hoelzle and Gruber, 2008; Schneider et al., 2012; Zhang, 2005), are represented in the regression result by rather small deviations of less than 1 K (Figure 8).
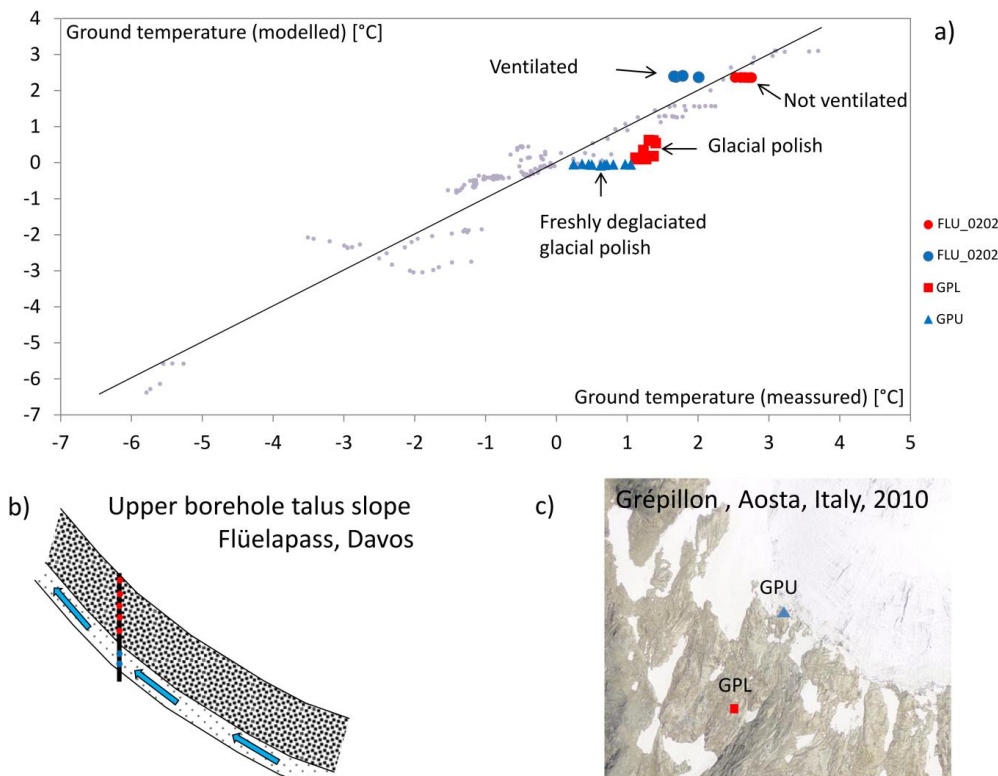
Figure 8: The Flüela- (Eastern Swiss Alps) and Grépillon (Italian Alps) boreholes show examples of thermal disturbances. The lowermost 3 thermistors in Flüela (FLU_0202) are ventilated (Phillips et al., 2009) and thus deviate from the regression line. The Grépillon boreholes are drilled in a glacial polish, which can warm more efficiently than the talus surfaces at most of the other boreholes. The upper Grépillon borehole (GPU) was only recently deglaciated: whereas the uppermost thermistors have adapted to the new thermal conditions, there is a clear temperature gradient towards lower temperatures at greater depth. Here, the temperatures are still close to 0° C as a consequence of the former glaciation.

Nevertheless, deviations exist due to advective cooling (Flüelapass; Figure 8a & 8b; (Phillips et al., 2009)), substrate characteristics (relatively warm glacial polish at the lower Grépillon borehole; Figure 8a & 8c) or

15
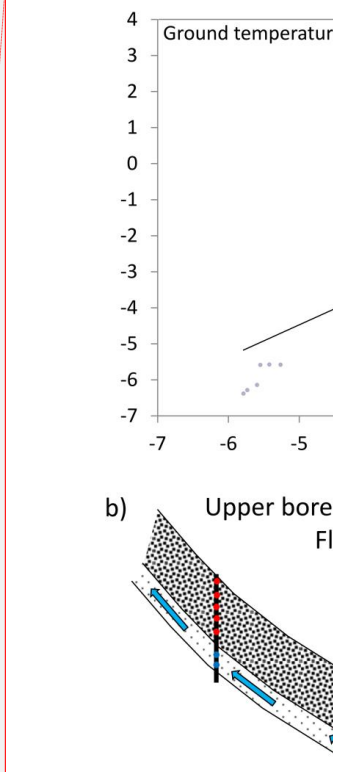
Gelöscht: 7

Gelöscht:

Gelöscht: 7

Gelöscht: 7a & 7b

Gelöscht: 7a % 7c) or temperature disturbances due to former glaciation (upper Grépillon borehole; Figure 7a & 7c).

temperature disturbances due to former glaciation (upper Grépillon borehole; Figure 8a & 8c). Additional deviations might arise from the climate warming signal in the borehole temperatures. While near-surface temperatures might be in accordance with the current climatic conditions, temperatures at greater depth are still influenced by previous decades with colder climate conditions. As temperatures at several depths are included in our reference data set, depth-dependent deviations can occur. Our model for ice-poor permafrost does thus not represent a permafrost distribution which is in equilibrium with the current climate conditions but a snapshot of the current distribution of ice-poor permafrost, which is currently adapting to warmer climate conditions.

Ice-rich permafrost cannot be satisfactorily predicted based on surface energy fluxes and requires the consideration of mass wasting processes such as rock fall and avalanche activity, as well as creep rates and varying glaciation during the Holocene. As these processes are often not known in detail, the accuracy of the cartographic representation of ice-rich permafrost is limited, as discussed in section 4.3.

4.2 Map uncertainty and accuracy

The uncertainty of a map can be quantified by the validation points, which are clearly mapped as being permafrost or not. In the PGIM, definitive permafrost is indicated by the core area of zone 1. In the APIM definitive permafrost is indicated by a permafrost index of 1 (for validation, values higher than 0.994 were rounded to 1). The PPDM does not have a zone of definitive permafrost. Definitive permafrost absence is indicated on all three maps for areas outside the permafrost zonation. The PGIM could attribute 69% of the validation points to a definitive class, while the APIM reached 33% and the PPDM 23% (Figures 5-7).

Accuracy can be measured by the number of validation points wrongly attributed to a definitive class or by the plausibility of the description of a class. In the PPDM, 7 permafrost sites occur outside the permafrost zonation. The definitive permafrost classes of the APIM and the PGIM predict all validation points correctly - with the exception of one site (Emshorn-Oberems), which is wrongly attributed on both maps. A weakness of our accuracy analysis is that the landforms and geographical locations of the validation sites do not represent the natural variability. Terrain- or region related errors of the permafrost zones, which are not captured in this accuracy analysis are therefore possible.

The APIM includes almost all areas in Switzerland in which permafrost will occur and is therefore a useful tool to exclude permafrost at a certain location. However, similar to the PPDM it shows weaknesses in the reproduction of permafrost-free areas, while the PGIM performs better here. This might be caused by the 'elevational permafrost gap' phenomenon introduced in section 1. Figure 9a shows the example of the research site Flüelapass (Kenner et al., 2017), with a permafrost-free belt between the ice-poor and ice-rich zones.

Mapping solely based on thermal influences is not able to reproduce the permafrost gap and either neglects the ice-rich permafrost at the base of talus slopes (Figure 9b) or overestimates the permafrost further upslope (Figure 9b and 9c). This problem leads to a high number of permafrost-free validation points in the zones of medium permafrost probability on the comparison maps; for example in the 60-70 % probability zone on the APIM or the zone "local permafrost possible, patchy to extensive" on the PPDM (Figures 6 and 7). This may also cause the rather random distribution of permafrost-free validation points over the remaining probability classes of the APIM. In the PGIM the permafrost gap becomes visible when plotting the mapped permafrost area against

16

Gelöscht: 4-6

Gelöscht: 8a

Gelöscht: 8b

Gelöscht: 8b
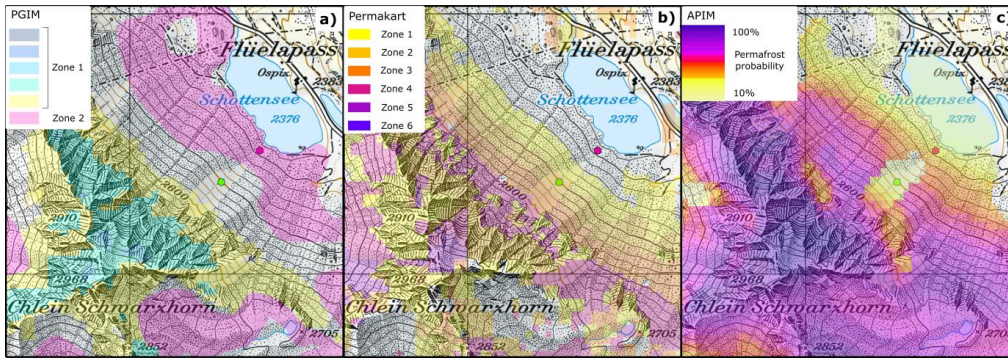
Gelöscht: 8c

Gelöscht: . For

Gelöscht: ,

Gelöscht: 5

Gelöscht: 6

elevation as shown in Figure D (supplementary material). A more accurate identification of this permafrost gap is an important step because it enables a better planning of ice-sensitive infrastructure in alpine terrain.

Gelöscht: C

Figure 9: Comparison of three permafrost maps at the research site Flüelapass (a: PGIM, b: PPDM (Gruber et al. 2006), c: APIM (Boeckli et al. 2012)). This example shows typical alpine permafrost distribution, with ice-rich permafrost at the base of a talus slope, a permafrost gap further upslope and permafrost in the rock wall above the talus slope. A borehole without permafrost (green dot (FLU_0202)) is located in the permfrost gap, another with ice-rich permafrost (pink dot (FLU_0102)) is at the base of the slope. (Map: pixmaps © (2017) swisstopo (5704 000 000))

Gelöscht: 8

4.3 Challenges and possible future approaches in mapping ice-rich permafrost

Zone 2 of the PGIM has a relatively high uncertainty. The low number of permafrost-free validation points wrongly attributed to this zone (2 out of 33, see Figure 5) might rather overestimate the accuracy of the zone due to a general lack of permafrost-free validation points in talus slopes. However, there is very little ice-rich permafrost outside this zone, as indicated by the 95% representation of the Albula rock glacier inventory within the automatically created raw version of zone 2. Accordingly, zone 2 should not be interpreted as a reliable representation of ice-rich permafrost but rather as a best-guess including most of the ice-rich permafrost in Switzerland, with some bycatch of permafrost-free ground. The greatest challenges in mapping ice-rich permafrost are the correct representation of rock glaciers and the differentiation between loose rock sediments, which can contain ice-rich permafrost and bedrock, which cannot. Merging existing, manually created rock glacier inventories in Switzerland to a nationwide inventory would improve zone 2 as the model approach could be focussed on ice-rich talus slopes.

Gelöscht: 4

Kenner and Magnusson (2017) highlighted the influence of the combined effect of lithology and precipitation on the occurrence of ice-rich permafrost: Ice-rich permafrost is less frequent in sedimentary rock areas with high precipitation rates and relatively abundant in drier areas with crystalline or metamorphic lithology. These regional climate- and lithology induced differences are difficult to implement in a map and must be carefully interpreted by the user.

17

4.4 Relevance of information on ground temperatures and ice content

The PGIM is the first large scale permafrost map indicating permafrost temperature and ground ice content. The ice-rich permafrost in Zone 2, located in lower elevations than zone 1, typically has temperatures at or slightly below 0°C (PERMOS, 2016). Knowledge of the distribution of ice-rich and/or warm permafrost is particularly important for engineering purposes, as ice affects the ground stability and bearing capacity strongest and should therefore be avoided during the infrastructure planning phase (Bommer et al., 2010). The construction of infrastructure on ice-rich permafrost can lead to destabilization of infrastructure through subsidence or creep induced by ice warming or even melting beneath the infrastructure. Construction activity and the subsequent use of infrastructure can lead to rapid changes in hydrology and ice content (Duvillard et al., 2019). The hydration heat of concrete and heat from machinery in buildings are particularly problematic if the permafrost contains ice (Phillips et al., 2007). Permafrost in rock walls is very sensitive to climate fluctuations (Noetzli and Gruber, 2009) and rock temperatures influence rock slope instability (Davies et al., 2001; Gruber and Haeberli, 2007; Krautblatter et al., 2013). In general, substrates with negative ground temperatures require specially adapted construction materials to prolong the service-life of infrastructure (Bommer et al., 2008).

4.5 Application to other regions

The mapping approach of zone 1 can probably be adapted to other mountain regions or future climate scenarios without requiring any local ground temperature reference data. Formula 4 in section 2.1 defines the distribution of ice-poor permafrost solely by the parameters PISR and elevation as a proxy for MAAT. PISR can be calculated globally based on digital elevation models. By setting radiation to 0, Formula 4 represents a direct conversion between elevation and MAAT. If the elevational MAAT distribution is known, elevation models for other climate regions can be adapted using this conversion and can then be used in the regression formula defined in this study. As for different climate regions, the elevation models can also be adapted to future scenarios of air temperatures. However, when adapting our results to a different climate, the transient effects have to be considered. As explained in 4.1., our model represents the actual current permafrost distribution in the Swiss Alps and is therefore not in equilibrium with the current climate. This disequilibrium might be smaller or larger in future or in different world regions. The performance of our regression formula for permafrost temperatures in other world regions should be tested in a future study using the validation dataset of worldwide borehole temperatures. This validation dataset is currently in preparation (ESA, 2018). This universal application of our method would only be feasible for mapping ice-poor permafrost. Our approach for modelling ice-rich permafrost can only be used for regions very similar to the Swiss Alps, as it is designed for non-arid, vegetated areas and requires special datasets such as information on past glaciation.

5 Conclusions

This study presents a new approach to map permafrost distribution in the Swiss Alps based on the differentiation of ice-poor and ice-rich permafrost. The new approach highlights i) the high predictability of ice-poor, thermally induced permafrost based on a simplified surface energy balance and ii) the need for a different mapping

18

Gelöscht: The

Gelöscht: it

Gelöscht: permafrost requires

Gelöscht: The same applies

Gelöscht: approach

Gelöscht: , and

approach for ice-rich permafrost typically formed at the base of slopes by alpine mass wasting. This is important for mapping and local modelling, but also to develop scenarios of present, past and future permafrost evolution.

We conclude that:

- Using a simple linear regression analysis of solar radiation and elevation, ground temperature profiles of 15 boreholes in ice-poor or ice-free ground could be modelled with a clearly sub-Kelvin accuracy.

- The regression result that zone 1 of the map is based on can easily be adapted to different climate conditions: either spatially for different mountain regions in the world, or temporally for future climate scenarios in Switzerland.

- A major improvement has been achieved in defining permafrost-free areas (referred to as a permafrost gap in this study), which can be of particular interest for construction projects involving ice-sensitive infrastructure.

- The distribution of ice-rich permafrost outside the continuous zone of permafrost is better predicted by the analysis of mass wasting processes than by thermal influencing factors.

- The permafrost and ground ice map PGIM presented contributes towards an improvement in the accuracy of permafrost mapping in Switzerland.

- The two zones on the map provide clear information on their meaning (i.e. ground temperatures versus the potential occurrence of excess ice permafrost) rather than a probability value, and are thus easy to interpret.

While the distribution of ice-poor permafrost is predictable with a high accuracy, there is a relatively large uncertainty referring to ice-rich permafrost. To improve the mapping result here, a more detailed dataset on surface characteristics (talus vs. bedrock) and manually mapped rock glacier inventories are required. An improved data base is needed as well for the validation of permafrost maps in general. Currently available datasets are biased regarding aspect, elevation and landforms. In addition, evidence of permafrost absence in the belt of discontinuous permafrost is clearly lacking.

19

Table 1: Reference boreholes provided by 1 - PERMOS (2016), 2 – WSL Institute for Snow and Avalanche Research SLF, 3 - Swiss Federal Office for the Environment FOEN, 4 - University of Lausanne, 5 - ARPA Valle d'Aosta. The uppermost 15 were used for the calculation of ground temperatures in zone 1 of the PGIM. The lowermost 8 were used to demonstrate the failure of this calculation if ice-rich and ice-poor boreholes are not distinguished (Table 3).

Line	Site name & provider	Abbreviation	Ground ice content	Elevation [m a.s.l.]	Longitude (WGS 84)	Latitude (WGS 84)	Time series
1	Breithorn [3]	BH	Ice-free	2865	7.81785	46.14010	2016 – 2017
2	Flüela 0202 [2]	FLU_0202	Ice-free	2501	9.94314	46.74687	2003 – 2005; 2009
3	Tsaté [1]	TSA_0104	Ice-poor	3040	7.54844	46.10904	2009 – 2012; 2015
4	Schilthorn 5200 [1]	SCH_5000	Ice-poor	2910	7.83442	46.55828	2006 – 2009; 2013 – 2015
5	Stockhorn 6000 [1]	STo_6000	Ice-poor	3410	7.82419	45.98678	2011 – 2012; 2014 – 2016
6	Les Attelas 3 [4]	ATT_0308	Ice-free	2741	7.27492	46.09659	2009 – 2010
7	Jungfrau [1]	JFJ_0195	Ice-poor	3590	7.97316	46.54617	2010 – 2015
8	Gemsstock [1]	GEM_0106	Ice-free	2940	8.61043	46.60125	2009 – 2010; 12; 15; 16
9	Cima Bianchi 41 [5] (Italy)	CB41	Ice-poor	3094	45.91906	7.69249	2010 – 2011; 2014 – 2017
10	Muot da Barba Peider 0196 [1]	MPB_0196	Ice-poor	2946	9.93109	46.49639	1997 – 2010; 2015 – 2016
11	Muot da Barba Peider 0296 [1]	MPB_0296	Ice-poor	2942	9.93143	46.49657	2000 – 2011; 2015; 2016
12	Cima Bianchi 7 [5] (Italy)	CB7	Ice-poor	3098	45.91920	7.69277	2010 – 2011; 2013 – 2017
13	Grépillon, upper [5] (Italy)	GPU	Ice-free	3047	7.05690	45.90990	2013 – 2017
14	Grépillon, lower [5] (Italy)	GPL	Ice-free	3000	7.05638	45.90919	2013 – 2017
15	Matterhorn [1]	MAT_0205	Ice-poor	3288	7.67605	45.98232	2006 – 2007; 2009 – 2013
16	Flüela 0102 [1]	FLU_0102	Ice-rich	2394	9.94516	46.74792	2005 – 2009; 2014
17	Attelas 0108 [1]	ATT_0108	Ice-rich	2661	7.27307	46.09677	2009 – 2010; 12; 15; 16
18	Attelas 0208 [1]	ATT_0208	Ice-rich	2689	7.27368	46.09674	2009 – 2010; 12; 15; 16
19	Corvatsch 0200 [1]	COR_0287	Ice-rich	2672	9.82185	46.42878	2001; 2003 – 2008; 2010; 2011 2013 – 2017
20	Lapires 1208 [1]	LAP_1108	Ice-rich	2500	7.28435	46.10611	2010; 2012; 2014
21	Muragl 0299 [1]	MUR_0299	Ice-rich	2539	9.92735	46.50722	2010 – 2013; 2016; 2017
22	Schafberg 0290 [1]	SBE_0190	Ice-rich	2754	9.92631	46.49737	2001 - 2016
23	Ritigraben 0102 [1]	RIT_0102	Ice-rich	2690	7.84983	46.17469	2003; 2004; 2006; 2007; 2009; 2012; 2014; 2016

Table 2: Validation sites and the zones assigned to them in the permafrost maps PGIM, APIM (Boeckli et al. 2012) and PPDM (Gruber et al. 2006). The bold typed sites at the bottom were used to set up the regression model for PGIM zone 1. Type: IMIS - IMIS station, BH - borehole, CS - construction site, RF - rock fall. Data providers: 1 – WSL Institute for Snow and Avalanche Research SLF, 2 - Cremonese et al. (2011), 3 - University of Lausanne, 4 – Swiss Federal Office for the Environment. 5 – University of Fribourg. Zones and probability classes of the maps: see Figures 5-7.

Gelöscht: 3-

Type[provider]	Name	Permafrost	PGIM/ Temp. (mod)	APIM	PPDM	Elevation [m a.s.l.]	Longitude (WGS 84)	Latitude (WGS 84)
IMIS [1]	Boveire - Pointe de Toules	No	Zone 2	43	Zone 4	2687	7.23722	45.98480
BH [3]	Lapir2	No	Zone 2	76	Zone 2	2559	7.28345	46.10526
IMIS [1]	Saas - Seetal	No	No perm.	No perm.	Zone 1	2477	7.87895	46.17137
IMIS [1]	Trubelboden - Trubelboden	No	No perm.	No perm.	No perm.	2459	7.58558	46.37096
IMIS [1]	Lukmanier - Lai Verd	No	No perm.	63	No perm.	2554	8.78352	46.60416
IMIS [1]	Fully - Grand Cor	No	No perm.	46	No perm.	2602	7.08964	46.19469
IMIS [1]	Bernina - Puoz Bass	No	No perm.	50	No perm.	2629	9.91588	46.44007
IMIS [1]	Gandegg - Gandegg	No	No perm.	72	No perm.	2710	7.76060	46.42926
IMIS [1]	Kesch - Porta d'Es-cha	No	No perm.	66	Zone 1	2727	9.89813	46.62132
IMIS [1]	Gornergrat - Gornergratsee	No	No perm.	98	Zone 5	2952	7.78359	45.98718
BH [2]	Barthélemy les Rochers (Zinal)	No	No perm.	35	Zone 2	2519	7.59812	46.13660
BH [2]	Neue Monte Rosa Hütte (Zermatt)	No	No perm.	93	Zone 1	2866	7.81233	45.95795
IMIS [1]	Zermatt - Alp Hermetje	No	No perm.	No perm.	No perm.	2409	7.70238	45.99799
IMIS [1]	Goms - Treichbode	No	No perm.	No perm.	No perm.	2428	8.22856	46.48912
IMIS [1]	Julier - Vairana	No	No perm.	No perm.	Zone 1	2426	9.69231	46.47850
IMIS [1]	Oberwald - Jostsee	No	No perm.	No perm.	No perm.	2432	8.31595	46.54522
IMIS [1]	Piz Martegnas - Colms da Prasonz	No	No perm.	No perm.	No perm.	2429	9.53739	46.58009
IMIS [1]	Bedretto - Cavanna	No	No perm.	No perm.	Zone 2	2420	8.51112	46.53268

20

IMIS[1]	Bernina - Motta Bianca	No	No perm.	No perm.	No perm.	2447	10.02920	46.42057
IMIS[1]	Davos - Hanengretji	No	No perm.	No perm.	No perm.	2456	9.77400	46.78885
IMIS[1]	Goms - Bodmerchumma	No	No perm.	10	Zone 2	2439	8.23251	46.42045
IMIS[1]	Taminatal - Wildsee	No	No perm.	59	No perm.	2468	9.39093	46.96836
IMIS[1]	Eggishorn - Flesch	No	No perm.	No perm.	No perm.	2500	8.09170	46.41680
IMIS[1]	Bever - Valetta	No	No perm.	No perm.	No perm.	2512	9.83713	46.53953
IMIS[1]	Samnaun - Ravaischer Salaas	No	No perm.	No perm.	No perm.	2512	10.33833	46.95637
IMIS[1]	Weissfluhjoch	No	No perm.	34	No perm.	2536	9.80911	46.82955
IMIS[1]	Les Attelas - Lac des Vaux	No	No perm.	No perm.	No perm.	2550	7.26988	46.10529
IMIS[1]	Davos - Barentalli	No	No perm.	No perm.	Zone 2	2557	9.81941	46.69890
IMIS[1]	Les Diablerets - Tsanfleuron	No	No perm.	65	No perm.	2584	7.23939	46.31445
IMIS[1]	Anniviers - Tracuit	No	No perm.	No perm.	No perm.	2589	7.65639	46.12116
IMIS[1]	Arolla - Breona	No	No perm.	No perm.	No perm.	2602	7.56205	46.08742
IMIS[1]	Anniviers - Orzival	No	No perm.	No perm.	Zone 4	2641	7.53536	46.18828
IMIS[1]	Zermatt - Triftchumme	No	No perm.	19	Zone 4	2753	7.72738	46.04217
CS[2]	Speichersee Totalpsee (Davos)	No	No perm.	26	Zone 2	2501	9.81109	46.83724
CS[2]	Herrenabfahrt Corviglia (St. Moritz)	No	No perm.	14	Zone 2	2829	9.80023	46.50610
BH[2]	Catogne (Bovernier)	No	No perm.	21	No perm.	2331	7.10474	46.06012
BH[2]	La Montagnetta (St. Jean/Grimentz)	No	No perm.	0	No perm.	2270	7.55943	46.19472
BH[2]	Barthélemy les Rochers (Zinal)	No	No perm.	0	Zone 2	2519	7.59812	46.13660
BH[2]	Barthélemy les Rochers (Zinal)	No	No perm.	0	Zone 1	2519	7.59812	46.13660
BH[2]	Emshorn (Oberems)	No	No perm.	16	Zone 1	2506	7.67602	46.26670
BH[2]	Emshorn (Oberems)	No	No perm.	0	No perm.	2506	7.67602	46.26670
BH[2]	Felskinnbahn (Saas Fee)	No	No perm.	68	Zone 2	2585	7.91784	46.08137
BH[2]	Illsee	No	No perm.	0	Zone 2	2359	7.63472	46.25945
BH[2]	Lapires	No	No perm.	97	Zone 4	2650	7.28345	46.10526
IMIS[1]	St. Niklaus - Oberer Stelligletscher	No	Zone 1: 0.4°C	86	Zone 2	2915	7.75054	46.16782
BH[5]	Attelas 3	No	Zone 1: 0.7°C	69	Zone 4	2741	7.27493	46.09660
IMIS[1]	Arolla - Les Fontanesses	No	Zone 1: 0.9°C	83	Zone 4	2857	7.44542	46.02967
IMIS[1]	Finhaut - L'Ecreuleuse	Yes	Zone 2	18	No perm.	2252	6.96409	46.10076
IMIS[1]	Simplon - Wenghorn	Yes	Zone 2	46	No perm.	2424	8.04516	46.17802
IMIS[1]	Piz Lagrev - Tscheppa	Yes	Zone 2	72	Zone 1	2727	9.74488	46.45112
IMIS[1]	Vinadi - Alpetta	Yes	Zone 2	82	Zone 5	2729	10.44286	46.93178
IMIS[1]	Saas - Schwarzmies	Yes	Zone 2	91	Zone 5	2799	7.97436	46.12436
CS[2]	Gruobtagfeld (Turtmanntal)	Yes	Zone 2	21	No perm.	2375	7.71797	46.20474
CS[2]	Wasserscheide (Davos Parsenn)	Yes	Zone 2	56	Zone 4	2620	9.80255	46.83391
BH[2]	Gentianes	Yes	Zone 2	87	Zone 5	2894	7.30226	46.08383
BH[2]	Mont Dolin (Arolla)	Yes	Zone 2	49	Zone 4	2597	7.46188	46.02634
BH[2]	Mont Dolin, (Arolla)	Yes	Zone 2	30	No perm.	2574	7.46330	46.02634
BH[2]	Ritigraben (Grächen)	Yes	Zone 2	51	Zone 4	2639	7.84983	46.17470
BH[2]	Seetalhorn (Grächen)	Yes	Zone 2	92	Zone 5	2862	7.85911	46.17642
BH[2]	Stafel-Seetalhorn (Grächen)	Yes	Zone 2	36	Zone 4	2457	7.86022	46.18694
BH[2]	Flüelapass (Davos)	Yes	Zone 2	29	No perm.	2500	9.94317	46.74688
BH[2]	Lapires	Yes	Zone 2	61	Zone 2	2505	7.28435	46.10612
BH[2]	Schafberg I	Yes	Zone 2	74	Zone 4	2752	9.92701	46.49655
BH[2]	Schafberg II	Yes	Zone 2	61	Zone 1	2729	9.92387	46.49909
BH[2]	Murtèl-Corvatsch	Yes	Zone 2	83	Zone 1	2666	9.82186	46.42879
BH[2]	Muragl I	Yes	Zone 2	60	Zone 4	2536	9.92784	46.50757
BH[2]	Les Attelas1	Yes	Zone 2	47	Zone 4	2661	7.27308	46.09677
BH[2]	Les Attelas2	Yes	Zone 2	55	Zone 4	2689	7.27369	46.09675
BH[2]	Emshorn (Oberems)	Yes	No perm.	0	Zone 2	2506	7.67602	46.26670
BH[2]	Muot da Barba Peider, lower shoulder	Yes	Zone 1: -0.1°C	81	Zone 4	2791	9.92891	46.49583
RF[2]	Gemsstock (Andermatt)	Yes	Zone 1: -0.2°C	99	Zone 1	2911	8.61043	46.60125
RF[2]	Chrachenhorn (Davos Monstein)	Yes	Zone 1: -0.4°C	91	Zone 5	2830	9.81226	46.68836
BH[2]	Pointe du Tsaté	Yes	Zone 1: -0.4°C	94	Zone 5	3028	7.54696	46.10995
BH[2]	Lagalp (Berninapass)	Yes	Zone 1: -0.4°C	97	Zone 2	Restricted	Restricted	Restricted
RF[2]	Kärpf (Elm)	Yes	Zone 1: -0.6°C	74	Zone 4	2654	9.08917	46.91611
CS[2]	Scex Rouge (Les Diablerets)	Yes	Zone 1: -0.6°C	93	No perm.	Restricted	Restricted	Restricted
CS[2]	Diavolezza (Berninapass)	Yes	Zone 1: -0.6°C	98	Zone 5	2993	9.96948	46.40975
BH[2]	Schilthorn 51/98	Yes	Zone 1: -0.7°C	100	Zone 4	2910	7.83462	46.55828
CS[2]	Cabane des Vignettes (Arolla)	Yes	Zone 1: -0.9°C	89	Zone 1	3164	7.47555	45.98865
CS[2]	Rothornhütte (Zermatt)	Yes	Zone 1: -0.9°C	98	Zone 4	Restricted	Restricted	Restricted
CS[2]	Rifugio Camosci (Pizzo Cristallina)	Yes	Zone 1: -0.9°C	94	No perm.	2903	8.53667	46.46444
BH[2]	Arolla, Mt. Dolin	Yes	Zone 1: -1.0°C	99	Zone 5	2862	7.45473	46.02663
BH[2]	Wisse Schijen (Randa)	Yes	Zone 1: -1.2°C	89	Zone 4	3039	7.74832	46.09635
BH[2]	Stockhorn 61/00	Yes	Zone 1: -2.7°C	100	Zone 4	3412	7.82420	45.98679
CS[2]	Cabane Dent Blanche (Ferpècle)	Yes	Zone 1: -3.3°C	100	Zone 2	Restricted	Restricted	Restricted
BH[2]	Jungfraujoch South	Yes	Zone 1: -3.9°C	100	Zone 2	3574	7.97306	46.54548
BH[2]	Jungfraujoch North	Yes	Zone 1: -5.2°C	100	Zone 4	3602	7.97319	46.54611
BH[2]	Eggishorn (Fiesch)	Yes	Zone 1: 0.6°C	88	Zone 1	2847	8.09365	46.42638
BH[2]	**Flüelapass 0202**	**No**	**No perm.**	**18**	**Zone 2**	**2500**	**9.94317**	**46.74688**
BH[2]	**Gemsstock**	**No**	**Zone 1: 0.4°C**	**97**	**Zone 2**	**2940**	**8.61043**	**46.60125**
BH[2]	**Les Attelas 3**	**No**	**No perm.**	**73**	**Zone 4**	**2741**	**7.27492**	**46.09659**
BH[4]	**Breithorn**	**No**	**Zone 1: 0.7°C**	**81**	**Zone 2**	**2864**	**7.81785**	**46.14010**
BH[2]	**Muot da Barba Peider I**	**Yes**	**Zone 1: -1.0°C**	**99**	**Zone 6**	**2938**	**9.93092**	**46.49647**
BH[2]	**Tsate**	**Yes**	**Zone 1: -1.0°C**	**96**	**Zone 2**	**3040**	**7.54844**	**46.10904**
BH[2]	**Schildhorn 5200**	**Yes**	**Zone 1: -0.3°C**	**100**	**Zone 4**	**2910**	**7.83442**	**46.55828**
BH[2]	**Stockhorn 6000**	**Yes**	**Zone 1: -2.8°C**	**100**	**Zone 5**	**3410**	**7.82419**	**45.98678**
BH[2]	**Jungfrau**	**Yes**	**Zone 1: -5.3°C**	**100**	**Zone 6**	**3590**	**7.97316**	**46.54617**
BH[2]	**Hörnligrat (Matterhorn, Zermatt)**	**Yes**	**Zone 1: -2.0°C**	**100**	**Zone 6**	**3288**	**7.67605**	**45.98232**

Table 3: Results of the regression analysis on ground temperature in dependency of elevation and PISR. Left: Regression analysis used to map the PGIM. Centre: Regression analysis using only the 'coldest thermistor' in boreholes in homogeneous terrain (no ridges). Right: Same approach as in the central column but including the ice-poor boreholes shown in table 1.

	Ice-poor permafrost (213 thermistors in 15 boreholes)	Ice-poor permafrost (coldest thermistor of 10 boreholes)	Ice-poor and ice-rich permafrost together (coldest thermistor of 10 ice-poor and 8 ice-rich boreholes)
Correlation coefficient	0.944	0.998	0.523
Standard error	0.57° C	0.16° C	1.02° C

22

References

Azócar Sandoval, G., Brenning, A., and Bodin, X.: Permafrost Distribution Modeling in the Semi-Arid Chilean Andes, 877-890 pp., 2017.

Böckli, L., Brenning, A., Gruber, S., and Noetzli, J.: Permafrost distribution in the European Alps: calculation and evaluation of an index map and summary statistics, The Cryosphere, 6, 807-820, 10.5194/tc-6-807-2012, 2012.

Böckli, L.: Characterizing permafrost in the entire European Alps: spatial distribution and ice content, University of Zurich, Mathematisch-naturwissenschaftliche Fakultät., 2013.

Bommer, C., Keusen, H.-R., and Phillips, M.: Engineering solutions for foundations and anchors in mountain permafrost, 9th International Conference on Permafrost, Fairbanks, Alaska, 2008, 159-163,

Bommer, C., Phillips, M., and Arenson, L. U.: Practical recommendations for planning, constructing and maintaining infrastructure in mountain permafrost, Permafrost and Periglacial Processes, 21, 97-104, 10.1002/ppp.679, 2010.

Cremonese, E., Gruber, S., Phillips, M., Pogliotti, P., Boeckli, L., Noetzli, J., Suter, C., Bodin, X., Crepaz, A., Kellerer-Pirklbauer, A., Lang, K., Letey, S., Mair, V., Morra di Cella, U., Ravanel, L., Scapozza, C., Seppi, R., and Zischg, A.: Brief Communication: "An inventory of permafrost evidence for the European Alps", The Cryosphere, 5, 651-657, 10.5194/tc-5-651-2011, 2011.

Davies, M. C. R., Hamza, O., and Harris, C.: The effect of rise in mean annual temperature on the stability of rock slopes containing ice-filled discontinuities, Permafrost and Periglacial Processes, 12, 137-144, 2001.

Deluigi, N., Lambiel, C., and Kanevski, M.: Data-driven mapping of the potential mountain permafrost distribution, Science of The Total Environment, 590, 370-380, 2017.

Duvillard, P.-A., Ravanel, L., Marcer, M., and Schoeneich, P.: Recent evolution of damage to infrastructure on permafrost in the French Alps, Regional Environmental Change, 19, 1281-1293, 10.1007/s10113-019-01465-z, 2019.

Ebohon, B., and Schrott, L.: Modeling Mountain Permafrost Distribution. A new Permafrost Map of Austria, Ninth International Conference on Permafrost, Fairbanks, Alaska, 2008, 397 - 402,

ESA: Permafrost CCI Project: http://cci.esa.int/Permafrost, access: 04.03.2019, 2018.

Fiddes, J., Endrizzi, S., and Gruber, S.: Large-area land surface simulations in heterogeneous terrain driven by global data sets: application to mountain permafrost, The Cryosphere, 9, 411-426, 10.5194/tc-9-411-2015, 2015.

Gisnås, K., Etzelmüller, B., Lussana, C., Hjort, J., Sannel, A. B. K., Isaksen, K., Westermann, S., Kuhry, P., Christiansen, H. H., Frampton, A., and Åkerman, J.: Permafrost Map for Norway, Sweden and Finland, Permafrost and Periglacial Processes, 28, 359-378, doi:10.1002/ppp.1922, 2017.

Gruber, S., and Hoelzle, M.: Statistical modelling of mountain permafrost distribution: local calibration and incorporation of remotely sensed data, Permafrost and Periglacial Processes, 12, 69-77, 2001.

Gruber, S., Hoelzle, M., and Haeberli, W.: Rock-wall temperatures in the Alps: modelling their topographic distribution and regional differences, Permafrost and Periglacial Processes, 15, 229-307, 2004.

Gruber, S., Haeberli, W., Krummenacher, B., Keller, F., Mani, P., Hunziker, G., Hölzle, M., Vonder Mühll, D., Zimmermann, M., Keusen, H.-R., A., G., and Rätzo, H.: Erläuterungen zur Hinweiskarte der potentiellen Permafrostverbreitung in der Schweiz 1:50'000, Swiss Federal Office for the Environment (FOEN), 2006.

Gruber, S., and Haeberli, W.: Permafrost in steep bedrock slopes and its temperature-related destabilization following climate change, Journal of Geophysical Research: Earth Surface, 112, 10.1029/2006JF000547, 2007.

Gruber, S.: Derivation and analysis of a high-resolution estimate of global permafrost zonation, The Cryosphere, 6, 221-233, 10.5194/tc-6-221-21012, 2012.

23

Haberkorn, A., Hoelzle, M., Phillips, M., and Kenner, R.: Snow as a driving factor of rock surface temperatures in steep rough rock walls, Cold Regions Science and Technology, 118, 64-75, 10.1016/j.coldregions.2015.06.013, 2015a.

Haberkorn, A., Phillips, M., Kenner, R., Rhyner, H., Bavay, M., Galos, S. P., and Hoelzle, M.: Thermal Regime of Rock and its Relation to Snow Cover in Steep Alpine Rock Walls: Gemsstock, Central Swiss Alps, Geografiska Annaler: Series A, Physical Geography, 97, 579-597, 10.1111/geoa.12101, 2015b.

Haeberli, W.: Untersuchungen zur Verbreitung von Permafrost zwischen Flüelapass und Piz Grialetsch (Graubünden). Mitteilungen der Versuchsanstalt für Wasserbau, Hydrologie und Glaziologie der ETH Zürich, Zurich, 221 pp., 1975.

Haeberli, W., Hoelzle, M., Dousse, J. P., Ehrler, C., Gardaz, J. M., Imhof, M., F., K., Kunz, P., R., L., and E., R.: Simulation der Permafrostverbreitung in den Alpen mit geographischen Informationssystemen, Schweizerischer Nationalfonds zur Förderung der wissenschaftlichen Forschung, 58, 1996.

Haeberli, W., and Vonder Mühll, D.: On the characteristics and possible origins of ice in rock glacier permafrost, Zeitschrift für Geomorphologie, 104, 43-57, 1996.

Haeberli, W.: Modern Research Perspectives Relating to Permafrost Creep and Rock Glaciers: A Discussion, Permafrost and Periglacial Processes, 11, 290-293, doi:10.1002/1099-1530(200012)11:4<290::AID-PPP372>3.0.CO;2-0, 2000.

Hilbich, C., Hauck, C., Hoelzle, M., Scherler, M., Schudel, L., Völksch, I., Vonder Mühll, D., and Mäusbacher, R.: Monitoring mountain permafrost evolution using electrical resistivity tomography: a 7-year study of seasonal, annual and long-term variations at Schilthorn, Swiss Alps, Journal of Geophysical Research, 113, 10.1029/2007JF000799, 2008.

Hipp, T., Etzelmüller, B., Farbrot, H., Schuler, T. V., and Westermann, S.: Modelling borehole temperatures in Southern Norway – insights into permafrost dynamics during the 20th and 21st century, The Cryosphere, 6, 553-571, 10.5194/tc-6-553-2012, 2012.

Hoelzle, M.: Permafrost occurrence from BTS measurements and climatic parameters in the Eastern Swiss Alps, Permafrost and Periglacial Processes, 3, 143-147, 1992.

Hoelzle, M., Haeberli, W., and Keller, F.: Application of BTS-measurements for modelling permafrost distribution in the Swiss Alps, 6th International Conference on Permafrost, Beijing, China, 1993,

Hoelzle, M., and Haeberli, W.: Simulating the effects of mean annual air-temperature changes on permafrost distribution and glacier size: an example from the Upper Engadin, Swiss Alps., Annals of Glaciology, 21, 399-405, 1995.

Hoelzle, M., Mittaz, C., Etzelmüller, B., and Haeberli, W.: Surface energy fluxes and distribution models of permafrost in European mountain areas: an overview of current developments, Permafrost and Periglacial Processes, 12, 53-68, 2001.

Hoelzle, M., and Gruber, S.: Borehole and ground surface temperatures and their relationship to meteorological conditions in the Swiss Alps, 2008.

Huete, A. R.: A soil-adjusted vegetation index (SAVI), Remote Sensing of Environment, 25, 295-309, 10.1016/0034-4257(88)90106-X, 1988.

Ishikawa, M.: Spatial mountain permafrost modelling in the Daisetsu Mountains, northern Japan, in: Permafrost, Eighth International Conference on Permafrost, Zurich, Switzerland, 2003, 020072388, 473-478,

Keller, F.: Automated mapping of mountain permafrost using the program PERMAKART within the Geographical Information Systems ARC/INFO, Permafrost and Periglacial Processes, 3, 133-138, 1992.

Keller, F., Frauenfelder, R., Gardaz, J. M., Hoelzle, M., Kneisel, M., Lugon, R., Phillips, M., Reynard, E., and Wenker, L.: Permafrost map of Switzerland, Seventh International Conference on Permafrost, Yellowknife Canada, 1998, 557-562,

Kenner, R., and Magnusson, J.: Estimating the effect of different influencing factors on rock glacier development in two regions in the Swiss Alps, Permafrost and Periglacial Processes, 28, 195-208, 10.1002/ppp.1910, 2017.

Kenner, R., Phillips, M., Hauck, C., Hilbich, C., Mulsow, C., Bühler, Y., Stoffel, A., and Buchroithner, M.: New insights on permafrost genesis and conservation in talus slopes based on observations at Flüelapass, Eastern Switzerland, Geomorphology, 290, 101-113, 10.1016/j.geomorph.2017.04.011, 2017.

Kenner, R.: Geomorphological analysis on the interaction of Alpine glaciers and rock glaciers since the Little Ice Age, Land Degradation & Development, doi:10.1002/ldr.3238, 2018.

Krautblatter, M.: Detection and Quantification of Permafrost Change in Alpine Rock Walls and Implications for Rock Instability, 2009.

Krautblatter, M., Funk, D., and Günzel, F. K.: Why permafrost rocks become unstable: a rock–ice-mechanical model in time and space, Earth Surface Processes and Landforms, 38, 876-887, 10.1002/esp.3374, 2013.

Lerjen, M., Kääb, A., Hoelzle, M., and Haeberli, W.: Local distribution of discontinuous mountain permafrost. A process study at Flüela Pass, Swiss Alps, Eighth International Conference on Permafrost, Zurich, 2003, 667-672,

Magnin, F., Deline, P., Ravanel, L., Noetzli, J., and Pogliotti, P.: Thermal characteristics of permafrost in the steep alpine rock walls of the Aiguille du Midi (Mont Blanc Massif, 3842 m a.s.l), The Cryosphere, 9, 109-121, 10.5194/tc-9-109-2015, 2015.

Maisch, M.: Die Gletscher der Schweizer Alpen: Gletscherhochstand 1850, aktuelle Vergletscherung, Gletscherschwund-Szenarien ; [Projektschlussbericht im Rahmen des Nationalen Forschungsprogrammes "Klimaänderungen und Naturkatastrophen", NFP 31], vdf, Hochsch.-Verlag an der ETH, 1999.

Maisch, M., Haeberli, W., Frauenfelder, R., Kääb, A., and Rothenbühler, C.: Lateglacial and Holocene evolution of glaciers and permafrost in the Val Muragl, Upper Engadin, Swiss Alps, in: Permafrost, edited by: Phillips, M., and Springman, S., A.A. Balkema Publishers, Lisse, 717-722, 2003.

Marmy, A., Salzmann, N., Scherler, M., and Hauck, C.: Permafrost model sensitivity to seasonal climatic changes and extreme events in mountainous regions, Environmental Research Letters, 8, 035048, 2013.

Noetzli, J., and Gruber, S.: Transient thermal effects in Alpine permafrost, The Cryosphere, 3, 85-99, 2009.

PERMOS: Permafrost in Switzerland 2010/2011 to 2013/2014, PERMOS, 85, 2016.

Phillips, M., Ladner, F., Müller, M., Sambeth, U., Sorg, J., and Teysseire, P.: Monitoring and reconstruction of a chairlift midway station in creeping permafrost terrain, Grächen, Swiss Alps, 47, 32-42, 10.1016/j.coldregions.2006.08.014, 2007.

Phillips, M., Zenklusen Mutter, E., Kern-Luetschg, M., and Lehning, M.: Rapid degradation of ground ice in a ventilated talus slope: Flüela Pass, Swiss Alps, Permafrost and Periglacial Processes, 20, 1-14, 10.1002/ppp.638, 2009.

Pogliotti, P.: Influence of snow cover on MAGST over complex morphologies in mountain permafrost regions, PhD thesis, Turin, Italy, Università degli Studi di Torino, 79 pp, 2011.

Pruessner, L., Phillips, M., Farinotti, D., Hoelzle, M., and Lehning, M.: Near-surface ventilation as a key for modeling the thermal regime of coarse blocky rock glaciers, Permafrost and Periglacial Processes, 29, 152-163, 2018.

Reynard, E., Lambiel, C., Delaloye, R., Devaud, G., Baron, L., Chapellier, D., Marescot, L., and Monnet, R.: Glacier/permafrost relationships in forefields of small glaciers (Swiss Alps), Proceedings 8th International Conference on Permafrost, Zurich, Switzerland, 2003, 947-952,

Ribolini, A., Guglielmin, M., Fabre, D., Bodin, X., Marchisio, M., Sartini, S., Spagnolo, M., and Schoeneich, P.: The internal structure of rock glaciers and recently deglaciated slopes as revealed by geoelectrical tomography: insights on permafrost and recent glacial evolution in

25

the Central and Western Alps (Italy–France), Quaternary Science Reviews, 29, 507-521, 10.1016/j.quascirev.2009.10.008, 2010.

Russi, T., Ammann, W., Brabec, B., Lehning, M., and Meister, R.: Avalanche Warning Switzerland 2000, in: Early Warning Systems for Natural Disaster Reduction, edited by: Zschau, J., and Küppers, A., Springer Berlin Heidelberg, Berlin, Heidelberg, 569-577, 2003.

Scapozza, C., Lambiel, C., Baron, L., Marescot, L., and Reynard, E.: Internal structure and permafrost distribution in two alpine periglacial talus slopes, Valais, Swiss Alps, Geomorphology, 132, 208-221, 10.1016/j.geomorph.2011.05.010, 2011.

Scherler, M., Hauck, C., Hoelzle, M., and Salzmann, N.: Modeled sensitivity of two alpine permafrost sites to RCM-based climate scenarios, Journal of Geophysical Research: Earth Surface, 118, 780-794, 10.1002/jgrf.20069, 2013.

Scherler, M., Schneider, S., Hoelzle, M., and Hauck, C.: A two-sided approach to estimate heat transfer processes within the active layer of the Murtèl–Corvatsch rock glacier, Earth Surf. Dynam., 2, 141-154, 10.5194/esurf-2-141-2014, 2014.

Schneider, S., Hoelzle, M., and Hauck, C.: Influence of surface and subsurface heterogeneity on observed borehole temperatures at a mountain permafrost site in the Upper Engadine, Swiss Alps, The Cryosphere, 6, 517-531, 10.55194/tc-6-517-2012, 2012.

Staub, B., Marmy, A., Hauck, C., Hilbich, C., and Delaloye, R.: Ground temperature variations in a talus slope influenced by permafrost: a comparison of field observations and model simulations, Geogr. Helv., 70, 45-62, 10.5194/gh-70-45-2015, 2015.

Zenklusen Mutter, E., and Phillips, M.: Active layer characteristics at ten borehole sites in Alpine permafrost terrain, Switzerland, Permafrost and Periglacial Processes, 23, 138-151, 10.1002/ppp.1738, 2012.

Zhang, T.: Influence of the seasonal snow cover on the ground thermal regime: an overview, Reviews of Geophysics, 43, 1-23, 2005.

26

a) First iteration
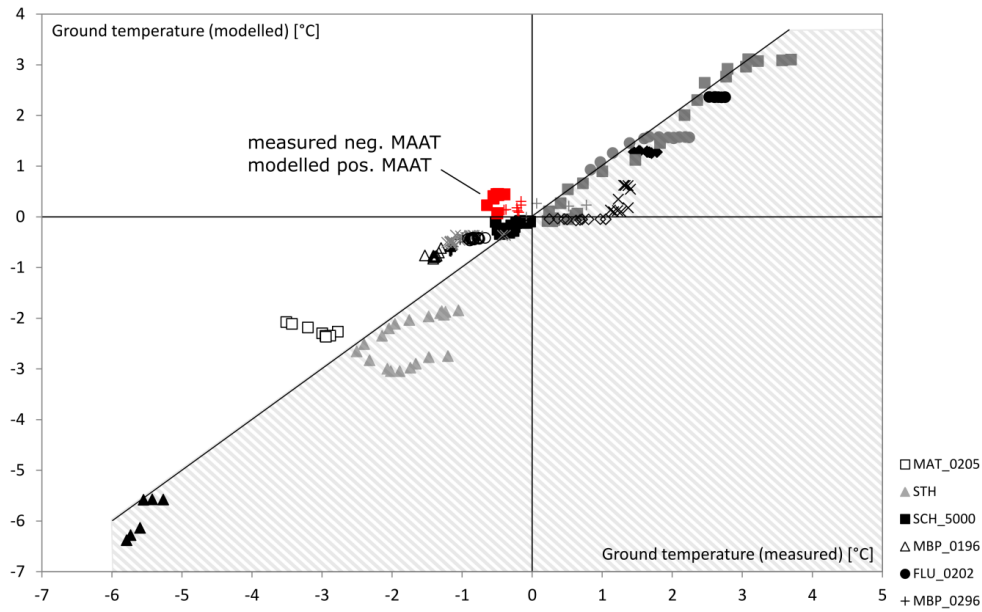
b) Second iteration
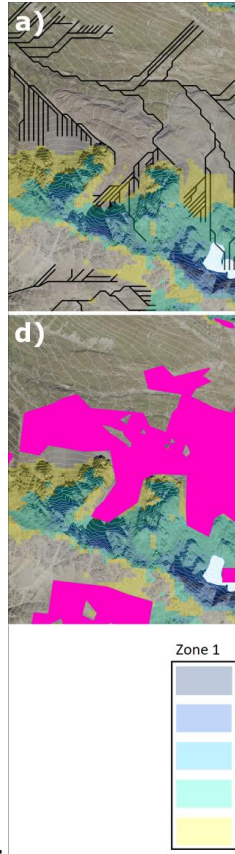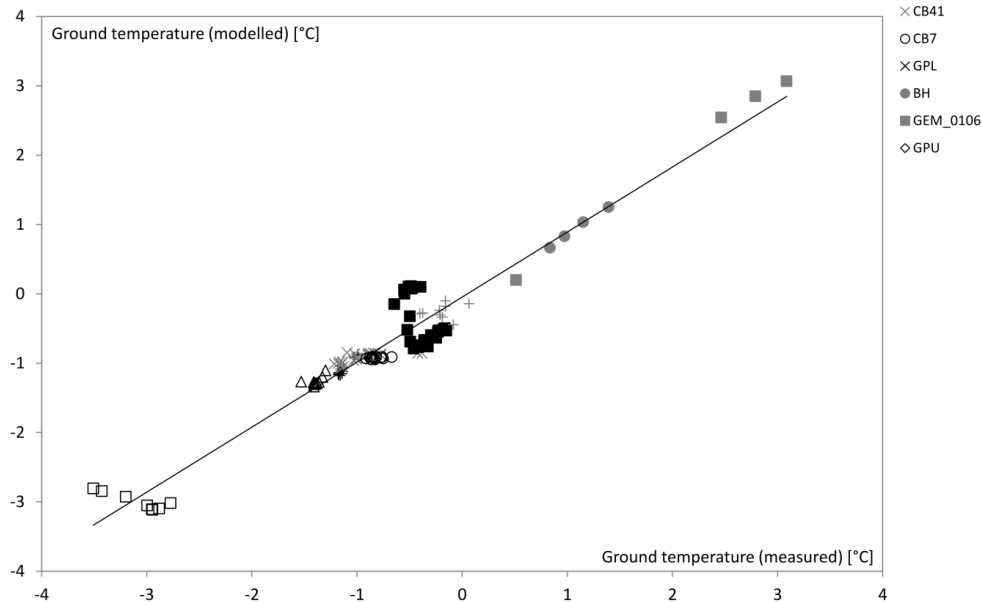
Gelöscht:
Figure A

Figure A: The initial regression result (part a) showed positive and negative deviations of the modelled temperatures compared to the measured ones. This can lead to positive modelled temperatures while negative temperatures are actually present. Transferred into the map this can cause the indication of permafrost absence while permafrost is actually present. To avoid this, all temperature measurements which lie above the modelled temperatures (i.e. all data points in the shaded area below the regression line) were not used in the second iteration (part b). The regression in

5
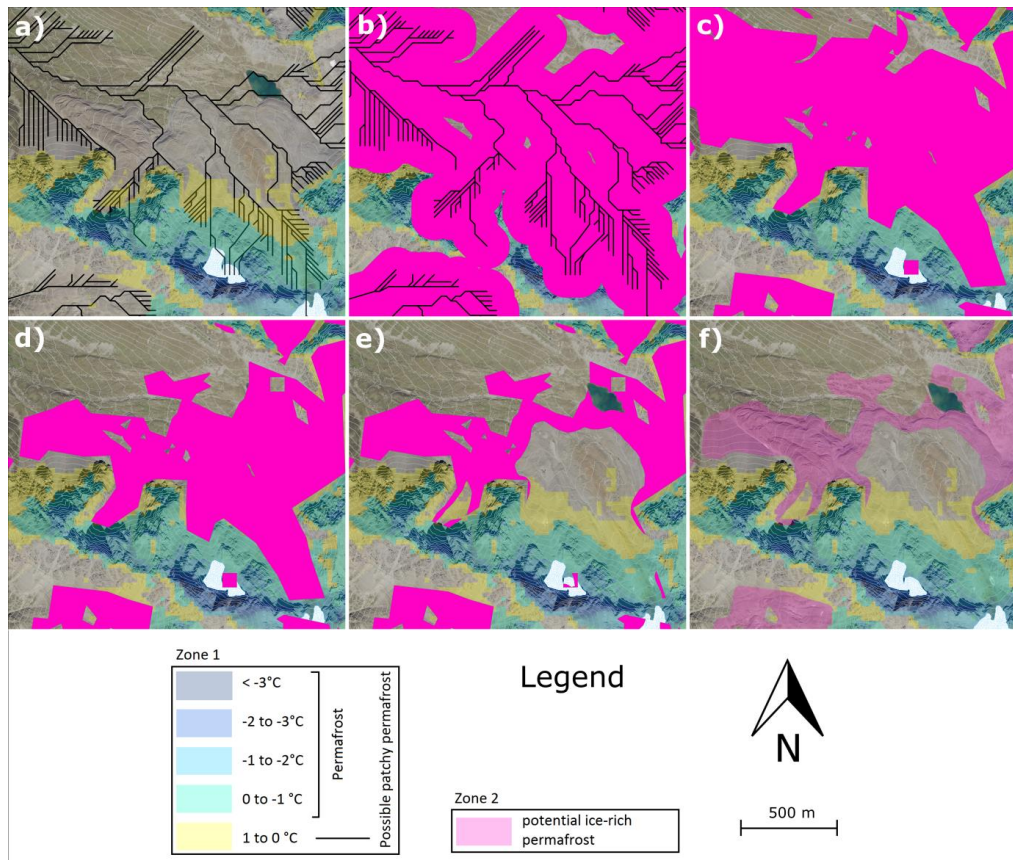
Figure B: Parts a-f show the individual work steps described in section 2.3 to create zone 2 representing ice-rich permafrost. The example shows the area around rock glacier Muragl (Kenner, 2018; Maisch et al., 2003). In short: a) Step 1: runoff tracks; b) Step 2: Buffered runoff tracks; c) Step 3: erase areas steeper 30°; d) Step 4: erase vegetated areas; e) Step 5+6: erase LIA glaciation & Lakes; f) Step 8: Simplified and smoothed output map.

10

Gelöscht: Simplifying

Gelöscht: smoothing

28
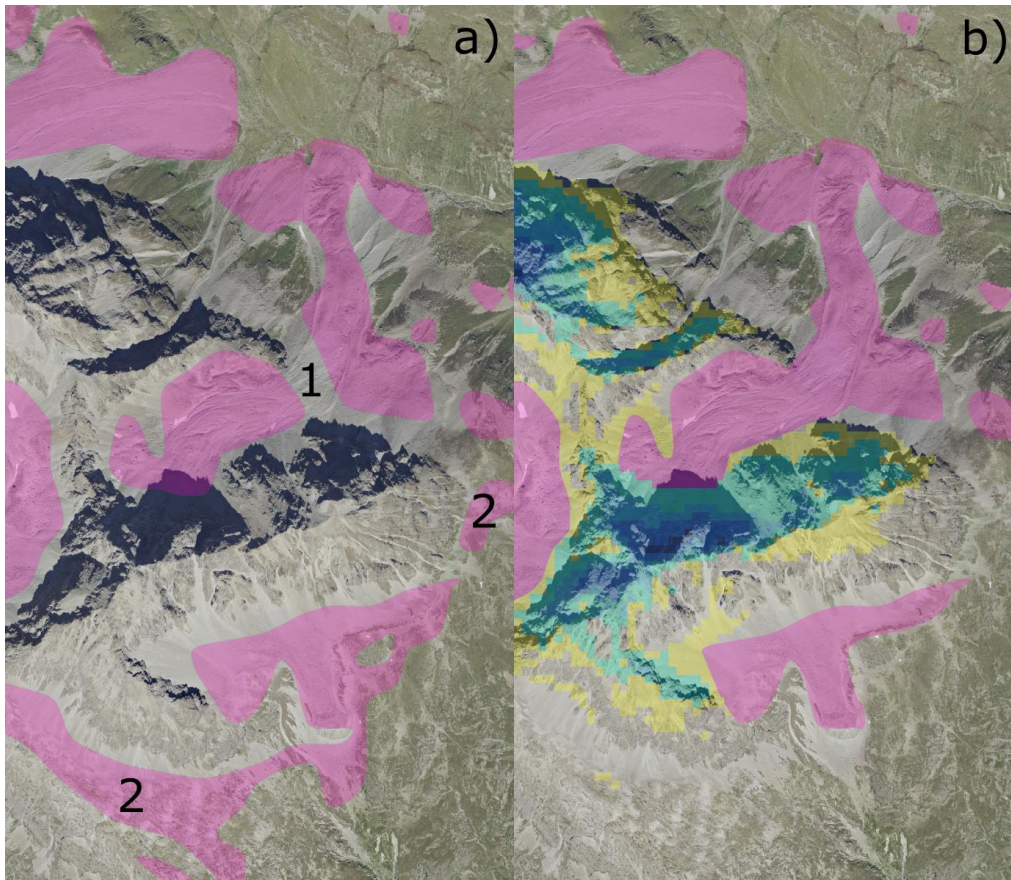
Figure C: Part a shows the raw model output for zone 2. Part b shows the edited zone 2 together with zone 1. Index 1 shows a part of the rock glacier which was not captured by the model due to a terrain step steeper than 30° and included manually. Index 2 shows zones which were manually removed as they mainly include bedrock or vegetation-covered ground.
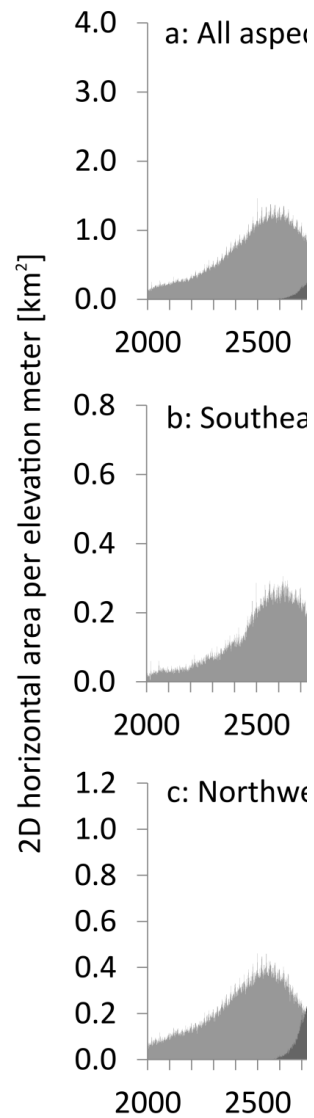
Figure C